



1 **LA Megacity: a High-Resolution Land-Atmosphere**
2 **Modelling System for Urban CO₂ Emissions**

3
4 **Sha Feng^{1,2*}, Thomas Lauvaux^{3,2}, Sally Newman⁴, Preeti Rao², Ravan**
5 **Ahmadov^{5,6}, Aijun Deng³, Liza I. Díaz-Isaac³, Riley M. Duren², Marc L.**
6 **Fischer⁷, Christoph Gerbig⁸, Kevin R. Gurney⁹, Jianhua Huang⁹, Seongeun**
7 **Jeong⁷, Zhijin Li², Charles E. Miller², Darragh O’Keeffe⁹, Risa Patarasuk⁹,**
8 **Stanley P. Sander², Yang Song⁹, Kam W. Wong^{4,2}, Yuk L. Yung⁴**

9
10 [1] JIFRESSE, University of California, Los Angeles, Los Angeles, CA

11 [2] Jet Propulsion Laboratory, California Institute of Technology, Pasadena, CA

12 [3] Department of Meteorology, Pennsylvania State University, College State, PA

13 [4] Division of Geological and Planetary Sciences, California Institute of Technology,
14 Pasadena, CA

15 [5] Cooperative Institute for Research in Environmental Sciences, University of Colorado
16 at Boulder, Boulder, CO

17 [6] Earth System Research Laboratory, National Oceanic and Atmospheric
18 Administration, Boulder, CO, USA

19 [7] Lawrence Berkeley National Laboratory, Berkeley, CA

20 [8] Max Planck Institute for Biogeochemistry, Hans-Knöll-Str.10, 07745 Jena, Germany

21 [9] Arizona State University, Tempe, AZ

22
23 [*] now at Department of Meteorology, Pennsylvania State University, University Park,
24 PA 16802, USA

25 Correspondence to: Sha Feng (sfeng@psu.edu)

26



1 **Abstract**

2 Megacities are major sources of anthropogenic fossil fuel CO₂ emissions. The spatial
3 extents of these large urban systems cover areas of 10,000 km² or more with complex
4 topography and changing landscapes. We present a high-resolution land-atmosphere
5 modelling system for urban CO₂ emissions over the Los Angeles (LA) megacity area.
6 The Weather Research and Forecasting (WRF)-Chem model was coupled to a very high-
7 resolution FFCO₂ emission product, Hestia-LA, to simulate atmospheric CO₂
8 concentrations across the LA megacity at spatial resolutions as fine as ~1 km. We
9 evaluated multiple WRF configurations, selecting one that minimized errors in wind
10 speed, wind direction, and boundary layer height as validated by its performance against
11 meteorological data collected during the CalNex-LA campaign (May-June 2010). Our
12 results show no significant difference between moderate- (4-km) and high- (1.3-km)
13 resolution simulations when evaluated against surface meteorological data, but the high-
14 resolution configurations better resolved PBL heights and vertical gradients in the
15 horizontal mean winds. We coupled our WRF configuration with the Vulcan 2.2 (10 km
16 resolution) and Hestia-LA (1.3-km resolution) fossil fuel CO₂ emission products to
17 evaluate the impact of the spatial resolution of the CO₂ emission products and the
18 meteorological transport model on the representation of spatiotemporal variability in
19 simulated atmospheric CO₂ concentrations. We find that high spatial resolution in the
20 fossil fuel CO₂ emissions is more important than in the atmospheric model to capture CO₂
21 concentration variability across the LA megacity. Finally, we present a novel approach
22 that employs simultaneous correlations of the simulated atmospheric CO₂ fields to
23 qualitatively evaluate greenhouse gas measurements over the LA megacity. Spatial
24 correlations in the atmospheric CO₂ fields reflect the coverage of individual measurement
25 sites when a statistically significant number of sites observe emissions from a specific
26 source or location. We conclude that elevated atmospheric CO₂ concentrations over the
27 LA megacity are composed of multiple fine-scale plumes rather than a single
28 homogenous urban dome. Furthermore, we conclude that FFCO₂ emissions monitoring in
29 the LA megacity requires FFCO₂ emissions modelling with ~1 km resolution since
30 coarser resolution emissions modelling tends to overestimate the observational
31 constraints on the emissions estimates.



1 1 Introduction

2 Carbon dioxide (CO₂) is a major anthropogenic contributor to climate change. It has
3 increased from its preindustrial (1750) level of 278 ± 2 ppm (Etheridge et al., 1996) to
4 over 400 ppm in recent years, as reported by the National Oceanic and Atmospheric
5 Administration (NOAA) and Scripps Institution of Oceanography [<http://co2now.org/>].
6 Clear evidence has shown that the continued increase of the atmospheric CO₂
7 concentration is dominated by global fossil fuel consumption during the same period
8 (IPCC, 2013) and land use change (Houghton, 1999).

9 Urban areas are significant sources of fossil fuel CO₂ (FFCO₂), representing more than
10 50% of the world's population and more than 70% of FFCO₂ (UN, 2006). In particular,
11 megacities (cities with urban populations greater than 10 million people) are major
12 sources of anthropogenic emissions, with the world's 35 megacities emitting more than
13 20% of the global anthropogenic FFCO₂, even though they only represent about 3% of
14 the Earth's land surface (IPCC, 2013). The proportion of emissions from megacities
15 increases monotonically with the world population and urbanization (UN, 2006, 2010).
16 Developed and developing megacities around the world are working together to pursue
17 strategies to limit CO₂ and other greenhouse gas (GHG) emissions (C40, 2012).

18 Carbon fluxes can be estimated using “bottom-up” and “top-down” methods. Typically,
19 FFCO₂ emissions are determined using “bottom-up” methods, by which fossil fuel usage
20 from each source sector is convolved with the estimated carbon content of each fuel type
21 to obtain FFCO₂ emission estimates. Space-time resolved FFCO₂ data sets using “bottom-
22 up” methods clearly reveal the fingerprint of human activity with the most intense
23 emissions being clustered around urban centres and associated power plants (e.g., Gurney
24 et al., 2009; Gurney et al., 2012). At the global and annual scale, FFCO₂ emission
25 estimates remain uncertain at ±5%, varying widely by country and reporting method (Le
26 Quéré et al., 2014). At the urban scale, the uncertainties of FFCO₂ emission estimates are
27 often 50-200 % (Turnbull et al., 2011; Asefi-Najafabady et al., 2014). “Top-down”
28 methods could potentially estimate biases in bottom-up emissions, and could also detect
29 trends that cities can use for decision-making, due to changing economic activity or
30 implementation of new emission regulations.



1 “Top-down” methods involve atmospheric measurements and usually include an
2 atmospheric inversion of CO₂ concentrations, using atmospheric transport models to
3 estimate carbon fluxes (i.e., posterior fluxes) by adjusting the fluxes (i.e., prior fluxes) to
4 be consistent with observed CO₂ concentrations (e.g., Lauvaux et al., 2012; Lauvaux et
5 al., 2015; Tarantola, 2005; Enting et al., 1994; Gurney et al., 2002; Baker et al., 2006;
6 Law et al., 2003). In general, a prior flux is required for estimating the fluxes using an
7 atmospheric inversion. The uncertainties in “top-down” methods therefore can be
8 attributed to errors in the observations (e.g., Tarantola, 2005), emission aggregation
9 errors from the prior fluxes (e.g., Gurney et al., 2012; Engelen et al., 2002), and physical
10 representation errors in the atmospheric transport model (e.g., Díaz Isaac et al., 2014;
11 Gerbig et al., 2008; Kretschmer et al., 2012; Lauvaux et al., 2009; Sarrat et al., 2007).
12 Previous studies showed that regional high-resolution models can capture the measured
13 CO₂ signal much better than the global models with lower resolution and simulate the
14 diurnal variability of the atmospheric CO₂ field caused by recirculation of nighttime
15 respired CO₂ well (Ahmadov et al., 2009). Pillai et al. (2011 and 2012) and Rödenbeck et
16 al. (2009) have discussed about the advantages of high resolution CO₂ modelling on
17 different domains and applications. Recent efforts to study FFCO₂ emissions on urban
18 scales have benefited from strategies that apply in-situ observations concentrated within
19 cities and mesoscale transport models (e.g., Wu et al., 2011; Lauvaux et al., 2015; Strong
20 et al., 2011; Lac et al., 2013; Bréon et al., 2015).

21 The Los Angeles (LA) megacity is one of the top three FFCO₂ emitters in the U.S. The
22 atmospheric CO₂ concentrations show complex spatial and temporal variability resulting
23 from a combination of large FFCO₂ emissions, complex topography, and challenging
24 meteorological variability (e.g., Brioude et al., 2013; Wong et al., 2015; Angevine et al.,
25 2012; Conil and Hall, 2006; Ulrickson and Mass, 1990; Lu and Turco, 1995; Baker et al.,
26 2013; Chen et al., 2013; Newman et al., 2013). Past studies of exploring CO₂
27 concentrations over the LA megacity used measurement methods ranging from ground-
28 based to airborne, from in-situ to column. Those studies consistently reported robust
29 enhancements (e.g., 30-100 ppm in-situ and 2-8 ppm column) and significant variability
30 of the CO₂ concentrations for the LA megacity (Newman et al., 2013; Wunch et al., 2009;
31 Wong et al., 2015; Kort et al., 2012; Wennberg et al., 2012; Newman et al., 2015). There



1 have been limited radiocarbon (^{14}C) isotopic tracer studies (Newman et al., 2013;
2 Newman et al., 2008; Djuricin et al., 2010; Riley et al., 2008; Newman et al., 2015).
3 Newman et al. (2013) showed that FFCO₂ constituted 10 - 25 ppm of the CO₂ excess
4 observed in the LA basin by averaging the flask samples at 1400 PST during 15 May –
5 15 June, 2010. Djuricin et al. (2010) demonstrated that fossil fuel combustion contributed
6 approximately 50~70 % of CO₂ sources in LA. Recently, using CO₂ mole fractions and
7 $\Delta^{14}\text{C}$ and $\delta^{13}\text{C}$ values of CO₂ in the LA megacity observed in inland Pasadena (2006–
8 2013) and coastal Palos Verdes peninsula (autumn 2009–2013), Newman et al. (2015)
9 demonstrated that fossil fuel combustion is the dominant source of CO₂ for inland
10 Pasadena. Airborne campaigns over LA (typically days to weeks in duration) included
11 ARCTAS-CA (Jacob et al., 2010) and CalNex-LA (Brioude et al., 2013). All of these
12 earlier studies were limited in their ability to investigate the spatial and temporal
13 characteristics of LA carbon fluxes given relatively sparse observations. To better
14 understand and quantify the total emissions, trends, and the detailed spatial, temporal, and
15 source sector patterns of emissions over the LA megacity requires both a denser
16 measurement network and a land-atmosphere modelling system appropriate for such a
17 complex urban environment. In this paper, we couple the Weather Research and
18 Forecasting (WRF) – Chem model to a high-resolution FFCO₂ emission product, Hestia-
19 LA, to study the spatiotemporal variability of urban CO₂ concentrations over the LA
20 megacity.

21 The mesoscale circulation over the LA megacity is challenging for atmospheric transport
22 models due to a variety of phenomena, such as “Catalina” eddies off the coast of southern
23 California and the coupling between the land-sea breeze and winds induced by the
24 topography (Angevine et al., 2012; Conil and Hall, 2006; Ulrickson and Mass, 1990;
25 Kusaka and Kimura, 2004b; Kusaka et al., 2001). In this paper we present a set of
26 simulations exploring WRF model physics configurations for the LA megacity,
27 evaluating the model performance against meteorological data from the CalNex-LA
28 campaign period, 15 May – 15 June 2010. Angevine et al. (2012) also investigated how
29 WRF model performance varied with spatial resolutions and PBL scheme, etc for the
30 CalNex-LA campaign period; however, Angevine et al. focused solely on model
31 meteorological evaluation with spatial resolutions of 12- and 4-km. In the present study



1 we focus on three critical aspects of the WRF model configuration – the planetary
2 boundary layer (PBL) scheme, the urban surface scheme, and the model spatial resolution
3 – as well as the effects of the FFCO₂ emissions product spatial resolution. Through these
4 four aspects, the impacts of physical representation errors and emission aggregation
5 errors on the modelled CO₂ concentrations across the LA megacity are investigated.

6 Moreover, a novel approach is proposed to evaluate the design of the greenhouse gas
7 (GHG) measurement network for the LA megacity. The LA measurement network
8 consists of 15 observation sites designed to provide continuous atmospheric CO₂
9 concentrations to assess the anthropogenic carbon emissions distribution and trends. The
10 goal of the network design exploration is to optimize the atmospheric observational
11 constraints on the surface fluxes. Kort et al. (2013) found that a minimum of eight
12 optimally located in-city surface CO₂ observation sites were required for accurate
13 assessment of CO₂ emissions in LA using the “footprint” method (backward mode) and
14 based on a national FFCO₂ emission product Vulcan. Here we assess the influence of
15 each observation site using spatial correlations in terms of the simulated CO₂ (forward
16 mode) at high-resolution.

17 The remainder of the paper is organized as follows. Section 2 describes the modelling
18 framework, including initial conditions and boundary conditions for WRF-Chem. In
19 section 3, we assess the quality of the model results, focusing on accurate representation
20 of the PBL height, wind speed and wind direction. Section 4 presents the spatial and
21 temporal patterns of simulated CO₂ concentration fields over the LA megacity using
22 various FFCO₂ emissions products. Section 5 describes the forward mode approach for
23 evaluating the spatial sensitivity of the 2015-era surface GHG measurement sites within
24 the LA megacity. Discussion of model errors, model sampling strategy, and the density of
25 the LA GHG measurement network from the forward model perspective is given in
26 section 6. A summary is given in section 7. Section 8 lists the author contributions.

27

28 **2 Modelling Framework**

29 Sensitivity experiments were conducted using WRF-Chem version 3.6.1 with various
30 PBL schemes, urban surface schemes, and model resolutions to define an optimized



1 configuration for simulating atmospheric CO₂ concentration fields over the LA megacity.
2 The impact of the resolution of FFCO₂ emission products is investigated as well.

3 **2.1 WRF model setup**

4 All of the model runs used one-way triple-nested domains with resolutions of 12-, 4-, and
5 1.3-km. The coarse domain (d01) covers most of the western US; the intermediate
6 domain (d02) covers California and part of Mexico (Figure 1a); the innermost domain
7 (d03) covers the majority of the South Coast Air Basin, a portion of the southern San
8 Joaquin Valley and extends into the Pacific Ocean to include Santa Catalina and San
9 Clemente Islands (Figure 1b). The Los Angeles basin is surrounded to the north and east
10 by mountain ranges with summits of 2-3 km, with the ocean to the west and the desert to
11 the north. The basin consists of the West Coast Basin, Central Basin, and Orange County
12 Coastal Plain. The boundaries of these three regions are Newport Inglewood Fault and
13 the boundary between Los Angeles County and Orange County. In this study, our
14 analysis is limited to the innermost domain (d03), referred to hereafter as the LA
15 megacity. All three of the model domains use 51 terrain following vertical levels from
16 surface to 100 hPa, of which 29 layers are below 2 km above ground level (AGL).

17 The meteorological fields and surface parameters, such as soil moisture, were initialized
18 by the three-hourly North American Regional Reanalysis (NARR) data set with a
19 horizontal resolution of 32 km (Mesinger et al., 2006) and the six-hourly NCEP sea
20 surface temperature data set with a horizontal resolution of 12 km
21 (<ftp://polar.ncep.noaa.gov/pub/history/sst/ophi>). A summary of WRF configurations
22 common to all sensitivity runs is shown in Table 1. The impact of varying the PBL
23 parameterization, urban surface, and model resolution was investigated by conducting
24 sensitivity runs summarized in Table 2.

25 PBL schemes are used to parameterize the unresolved turbulent vertical fluxes of heat,
26 momentum, and constituents within the planetary boundary layer. There are tens of
27 mesoscale PBL schemes available in the WRF package. We selected the three most
28 commonly used turbulent kinetic energy (TKE)-driven PBL schemes for the sensitivity
29 runs: the Mellor-Yamada-Janjic technique (MYJ, Janjić, 1994), Mellor-Yamada



1 Nakanishi and Niino Level 2.5 (MYNN, Nakanishi and Niino, 2006), and Bougeault-
2 Lacarrère (BouLac, Bougeault and Lacarrere, 1989). The TKE-driven PBL schemes
3 explicitly estimate the turbulent fluxes from mean atmospheric states and/or their
4 gradients and can be used to drive a Lagrangian particle dispersion models in subsequent
5 atmospheric inversions (e.g., Lauvaux et al., 2008).

6 For an accurate representation of the LA CO₂ simulation, the necessity of incorporating
7 the urban surface scheme was tested by alternatively including an urban canopy model
8 (UCM, Kusaka and Kimura, 2004a), a building environment parameterization (BEP,
9 Martilli et al., 2009), and no urban surface scheme.

10 We chose to test and evaluate our WRF-Chem configuration during the May-June 2010
11 time period of the CalNex-LA campaign (Ryerson et al., 2013) to take advantage of the
12 extra meteorological measurements recorded during the campaign. Hourly simulations
13 were conducted for 36-h periods starting with a 12-h meteorological spin-up at 12:00
14 UTC of the previous day. Hence, when concatenating the model output, each new run is
15 introduced at 0000 UTC. All of the analyses in the following sections are limited to the
16 region of the LA megacity.

17 **2.2 Configuration for the CO₂ simulation**

18 WRF-Chem version 3.6.1 was modified to allow for online CO₂ tracer transport coupled
19 with the Vegetation Photosynthesis and Respiration Model (VPRM) (Ahmadov et al.,
20 2007; Xiao et al., 2004). VPRM calculates hourly net ecosystem exchange based on
21 MOIDS satellite estimates of the land surface water index and enhance vegetation index,
22 short wave radiance and surface temperature. A detailed description of VPRM can be
23 found in Mahadevan et al. (2008).

24 Anthropogenic FFCO₂ fluxes were alternatively prescribed from the Vulcan 2.2 and
25 Hestia-LA 1.0 FFCO₂ emission products developed at Arizona State University (Gurney
26 et al., 2009; Gurney et al., 2012; Gurney et al., 2015; Rao et al., 2015). Both emission
27 products were developed using “bottom-up” methods. Vulcan quantifies FFCO₂
28 emissions for the entire contiguous United States (CONUS) hourly at approximately 10
29 km spatial resolution for the year of 2002, combining data sources such as local pollution



1 reporting, traffic data, and point source monitoring (Gurney et al., 2009). Hestia-LA, by
2 contrast, is a fossil fuel CO₂ emissions data product specific in space and time to the
3 individual building, road segments, and point sources of the Los Angeles megacity (Rao
4 et al., 2015; Gurney et al., 2015; Gurney et al., 2012; Zhou and Gurney, 2010).
5 Leveraging from the Vulcan constraint at the county level, Hestia-LA quantifies FFCO₂
6 emissions for Los Angeles County, Orange County, San Bernardino County, Ventura
7 County, and Riverside County, at approximately 1.3 km x 1.3 km every hour of the years
8 of 2011 and 2012. More details about Hestia-LA see Rao et al. (2015).

9 Atmospheric CO₂ concentrations in WRF-Chem were alternatively driven by the Vulcan
10 and Hestia-LA emissions at the resolutions of 4 km and 1.3 km. Hence, four different
11 emission datasets were generated – Vulcan 10 km emissions transported at 4-km or 1.3-
12 km resolution, and Hestia-LA 1.3 km emissions transported at 4-km or 1.3-km resolution.
13 The Hestia-LA emissions were aggregated from the native building-level resolution to
14 the 1.3 and 4 km resolutions via direct summation in the specified model grids. Hestia-
15 LA 2011 is temporally shifted for creating the weekday-weekend cycle for the year of
16 2010. The Vulcan FFCO₂ emissions were interpolated by using a bilinear operator and by
17 preserving the value of the integral of data between the source (10-km) and destination
18 (4- and 1.3-km) grid. Also, the ratio of the total carbon emissions over the state between
19 the years of 2002 and 2015 from California Air Resource Board (<http://www.arb.ca.gov/>)
20 was uniformly applied to the Vulcan emissions to temporally scale Vulcan from the 2002
21 base year to 2010. At regional scales, anthropogenic and biogenic fluxes are much larger
22 than ocean fluxes. Hence, no CO₂ ocean fluxes were prescribed. This paper analyses the
23 impact of both physical representation errors and emission aggregation errors on the
24 modelled CO₂ concentrations across the LA megacity.

25 Lateral boundary conditions and initial conditions for CO₂ concentration fields were
26 taken from the three-dimensional CO₂ background (often called “NOAA curtain” for
27 background) estimated from measurements in the Pacific (Jeong et al., 2013).

28



1 **3 Model – data comparison**

2 Meteorological observations obtained during the CalNex-LA campaign
3 (<http://www.esrl.noaa.gov/csd/projects/calnex/>) include PBL height sampled by NOAA
4 P-3 flights and aerosol backscatter ceilometer (Haman et al., 2012; Scarino et al., 2013), a
5 radar wind profiler operated by the South Coast Air Quality Management District near
6 Los Angeles International Airport (LAX), and CO₂ in situ measurements (Newman et al.,
7 2013). Additionally, the NWS (National Weather Service, www.weather.gov) surface
8 observations are used.

9 **3.1 Comparison to aircraft PBL height**

10 During CalNex-LA, 17 P-3 research flights sampled the daytime and nighttime PBL,
11 marine surface layer, and the overlying free troposphere throughout California (Ryerson
12 et al., 2013). We imposed five criteria for selecting aircraft profiles of potential
13 temperature for PBL height comparisons:

- 14 1) Aircraft profiles sample within the innermost model domain (d03, Figure 1b);
- 15 2) Profiles sample during daytime (1100 PST – 1700 PST) when the CO₂ concentrations
16 in PBL is well mixed;
- 17 3) Profiles acquired within ±30 min of the model output;
- 18 4) Profiles with valid sampling below and above 1 km AGL to assure the chance to
19 determine the PBL height from the potential temperature vertical gradient;
- 20 5) Ability to determine the PBL height from the vertical gradient of potential
21 temperature.

22 Based on these five criteria, we selected seven aircraft profiles collected between 16 May
23 and 19 May 2010. Figure 2 shows a profile acquired on 19 May 2010 when the aircraft
24 was sampling over Pasadena.

25 The model diagnostic PBL height calculated by each PBL scheme can differ from the
26 others due to the Richardson bulk number (R_b) used (e.g., Kretschmer et al., 2014; Hong
27 et al., 2006; Yver et al., 2013). To avoid this difference, we determined modelled PBL
28 height based on the vertical virtual potential temperature gradient. For the case (Figure



1 2), the modelled PBL height agrees within 50 meters of the aircraft-determined and
2 ceilometer-measured PBL height

3 Figure 3 shows the absolute difference between the modelled and aircraft-determined
4 PBL height for each selected aircraft profile. The differences between the modelled and
5 aircraft-determined PBL height differ case by case. None of the model physics is
6 systematically better than others. However, BouLac_BEP and MYNN have larger biases
7 than others. The averaged bias of BouLac_BEP is 289 m for d02, 295 m for d03; MYNN
8 is 179 m for d02 and 216 m for d03. For other configurations, the averaged biases are
9 smaller than 160 m. The modelled PBL bias appears somewhat smaller in the 4-km runs
10 than the 1.3-km runs. This, however, is obtained based on seven selected aircraft profiles
11 only. To further define the optimal physics for the PBL height simulation, we will present
12 the all-hours statistics with the ceilometer data in section 3.2.

13 **3.2 Comparison to ceilometer PBL height**

14 Accurate simulation of the time evolution of the PBL height is crucial to properly
15 simulate the vertical mixing and ventilation of CO₂ emitted at the surface. The ceilometer
16 measurements during CalNex-LA (Haman et al., 2012) allow us to evaluate the time
17 evolution of the modelled PBL height. Compared with the ceilometer-measured PBL
18 height, the maximum discrepancies between model and observations occur from around
19 1100 PST – 1200 PST when the nocturnal PBL is fully collapsed and 1700 PST when it
20 starts to form again (Figure 4). Among all of the model physics, MYNN_UCM shows the
21 best agreement with the observations, while BouLac_BEP differs from ceilometer the
22 most. The absolute bias of the MYNN_UCM modelled PBL height ranges from 5 to 198
23 m and 0 to 184 m with mean bias of -15.3 ± 66.1 m and -6.9 ± 82.7 m for d02 and d03,
24 respectively, suggesting the 1.3-km model resolution statistically improves the model
25 performance in the PBL simulation as compared with the ceilometer. The improvement
26 in the high-resolution model runs can be seen in other configurations as well. However,
27 the ceilometer measurements were all at Caltech and thus reflect interior conditions.
28 These are expected to be very different from coastal conditions in terms of the temporal
29 evolution and eventual height of the mid-day PBL as well as the timing of the nocturnal



1 PBL collapse, etc. The domain is much larger and more varied than captured by a single
2 location.

3 We also notice that using UCM-coupled simulations agree with the ceilometer better than
4 other combinations (MYNN_UCM vs. MYNN, MYJ_UCM vs. MYJ, BouLac_UCM vs.
5 BouLac_BEP). Using UCM can largely reduce the difference across the model runs and
6 discrepancy from the observations.

7 **3.3 Comparison to radar wind profiler**

8 Atmospheric dynamics has a direct influence on the CO₂ transport. Realistically
9 reproducing the vertical gradient of wind fields is crucial. In Figure 5, we show the
10 average difference in the wind profiles between the models and the radar wind profiler at
11 LAX (Angevine et al., 2012). Most of the simulations show relatively larger wind speed
12 bias near the surface: BouLac_BEP, MYJ, and MYNN with bias of 2.4 ± 2.2 m/s,
13 BouLac_UCM and MYJ_UCM with bias of 2.0 ± 2.3 m/s. In contrast, it is encouraging
14 to see that MYNN_UCM agrees with the radar measurement best with mean bias of $1.4 \pm$
15 2.0 m/s, a lower mean bias than for the other configurations. Additionally, UCM-coupled
16 simulations tend to reduce the wind speed bias at this location.

17 For wind direction, likewise, MYNN_UCM agrees with the observations slightly better
18 below 800 m (About 1.1 m/s for the averaged error), although the model bias is much less
19 pronounced across the configurations. However, we notice that MYNN_UCM shows
20 larger wind direction bias between 800 – 1400 m than others due to relatively lower PBL
21 height simulated (not shown).

22 Improvement provided by the 1.3-km model resolution is visible near the PBL height
23 (800 – 1400 m). A finer model resolution tends to resolve the vertical gradients of the
24 atmospheric states better. This also can be demonstrated by the PBL comparisons with
25 ceilometer (Figure 4).

26 Angevine et al. (2012) evaluated a set of model configurations with the highest model
27 resolution at 4 km for CalNex-LA using the same radar wind profiler data. The optimal
28 configuration (the total energy–mass flux boundary layer scheme and ECMWF
29 reanalysis) they found showed 1.1 ± 2.7 m/s bias in wind speed and $-2.6 \pm 67^\circ$ in wind



1 direction near the surface. Here MYNN_UCM displays similar performance to the
2 optimal configuration they concluded. At the 4-km model resolution, the biases of
3 MYNN_UCM are 1.4 ± 2.0 m/s in wind speed and $-1.3 \pm 20.0^\circ$ in wind direction. In
4 section 3.4, we will examine the performance of MYNN_UCM across the LA megacity.

5 **3.4 Comparison to NWS surface stations**

6 Due to the limited number of observation sites available at this time in this region, the
7 analysis above can only be done at specific locations. We therefore introduce the NWS
8 surface network to demonstrate the model performance across the LA megacity. The
9 objective analysis program OBSGRID is used to remove erroneous data and observations
10 that are not useful (Deng et al., 2009; Rogers et al., 2013).

11 Figure 6 shows the model bias compared to the NWS surface data across the LA
12 megacity. The locations of the GHG measurement sites are marked (see details in Table 3
13 and Figure S1). Overall, there is little difference in the simulated surface atmospheric
14 state variables between the 4-km and 1.3-km runs; i.e., the 1.3-km run does not show any
15 significant improvement compared to the 4-km run at the surface (even though it resolves
16 the vertical gradient of atmospheric states and PBL better, Figure 4 and 5).

17 For temperature (Figure 6a1 and 6b1), the model is colder than the observations by 0.5 -
18 1.0 K. Larger temperature biases occur in the desert. For relative humidity (Figure 6a2
19 and 6b2), the model is dry compared to the observations, which is consistent with the
20 findings of Nehr Korn et al. (2012). The model is 5% dryer over the basin with a
21 somewhat larger bias of 5% - 10% near Granada Hills and Ontario that have the highest
22 temperature in the summer – typically 20 °F or more warmer than downtown LA in May-
23 June. The dryness in the model tends to cause lower PBL heights, which can be seen in
24 the comparison to the ceilometer-determined PBL height at Caltech in Pasadena,
25 California (Figure 4): MYNN_UCM shows a shallower PBL in comparison to the
26 ceilometer during the 1400 PST – 1800 PST time period.

27 The model overestimates wind speed by ~ 1.0 m/s (Figure 6a3 and 6b3). The tendency of
28 the model to overestimate wind speed is fully documented in previous studies (e.g.,
29 Angevine et al., 2012; Brioude et al., 2013; Nehr Korn et al., 2012; Yver et al., 2013). For



1 surface wind direction, model bias is within $\pm 10^\circ$ for most of the LA megacity. The
2 larger biases appear near the foothills of Santa Monica Mountains, San Gabriel
3 Mountains, and University of Southern California (USC) due to the challenging land
4 surface and terrain.

5 Compared with other model physics (not shown), we notice that USC located in the
6 downtown LA is a challenging location for mesoscale modelling, in particular for wind
7 simulations. All of the model physics consistently show a relatively large wind bias at
8 USC except BouLac_BEP that fails in the remainder of the domain. We also noticed that
9 adding UCM to MYNN decreases the modelled temperature, while all of other models'
10 physics have a warm bias compared to observations.

11 All of the analyses above focused on the meteorology over the LA megacity. The results
12 indicate little difference horizontally between 4- and 1.3-km runs across the basin, which
13 is consistent with the Angevine et al. (2012) assumption that a finer grid may not give
14 better results. However, the 1.3-km run tends to resolve the vertical gradients of
15 atmospheric state variables and PBL better, which can improve the vertical mixing and
16 ventilation of modelled atmospheric CO₂ concentrations.

17 Overall, the MYNN_UCM configuration showed the best agreement with meteorological
18 observations of all the configurations we evaluated. Therefore, we will use the MYNN-
19 UCM configuration in our simulations of atmospheric CO₂ concentration fields over the
20 LA megacity.

21 **3.5 Comparisons to in-situ CO₂**

22 We coupled Hestia and Vulcan FFCO₂ emission products individually with the
23 MYNN_UCM WRF configuration to generate four sets of simulated CO₂ concentrations:
24 WRF-Hestia 1.3-km, WRF-Hestia 4-km, WRF-Vulcan 1.3-km, and WRF-Vulcan 4-km.
25 The runs with the same model resolution have the same meteorology but differ in
26 emissions, and vice versa.

27 During CalNex-LA, in-situ observation sites at Pasadena and Palos Verdes continuously
28 measured surface CO₂ concentrations. Measurements were recorded using a Picarro
29 (Santa Clara, CA) Isotopic CO₂ Analyser (cavity ring-down spectrometer), model G1101-



1 i, for Pasadena and an infrared gas analyser from PP Systems (Haverford, MA), model
2 CIRAS-SC for Palos Verdes. In addition, periodic flask samples were collected for
3 analysis of $^{14}\text{CO}_2$ for extracting fossil fuel and biogenic signals. See Newman et al.
4 (2015) for details about the sites and sampling information. Figure 7 shows the
5 comparison of the time series of hourly (Figure 7a,b) and daily afternoon (Figure 7c,d)
6 averaged CO_2 concentrations (1300 PST – 1700 PST) between model and observation.
7 Overall, the model captures the temporal variability of CO_2 but overestimates CO_2 during
8 nighttime. During afternoons, the model agrees with the observations fairly well (Figure
9 7c and 7d) except for a few events: all simulations underestimate CO_2 concentrations by
10 about 10 ppm around May 28 and June 4-6 for Pasadena and May 21 for Palos Verdes.
11 These events lasting two – three days are likely related to synoptic scale processes. Using
12 the averaged Pacific Ocean CO_2 signal as background may explain the failure to capture
13 these events. Further investigation of the background air would provide insights related to
14 synoptic variability but is beyond the scope of this work. We focus here on the diurnal
15 variability.

16 Clear diurnal variations of the surface CO_2 concentrations were observed for both sites
17 (Figure 8). The observed CO_2 concentrations increase at night and remains high until
18 sunrise, and quickly drop as the boundary layer grows after sunrise (Figure 8a and 8b).

19 For the Pasadena site, during nighttime, when the PBL is shallow, CO_2 is trapped locally:
20 the more fossil fuel is emitted, the higher CO_2 concentration is simulated. Consequently,
21 the WRF-Vulcan runs show considerably lower CO_2 concentration than the WRF-Hestia
22 runs due to the lower emissions in Vulcan at the Pasadena site (Figure 8c). However,
23 during daytime, with well-mixed conditions, the discrepancy between the WRF-Hestia
24 and WRF-Vulcan runs becomes smaller. Among these runs, the 1.3-km WRF-Hestia run
25 successfully captures the diurnal variation of the surface CO_2 concentration, although a
26 peak is not present in the observation around noon. By contrast, the 4-km WRF-Hestia
27 run underestimates the CO_2 concentration during 0200 – 0700 PST even though
28 emissions were comparable between Hestia 4-km and Hestia 1.3-km (Figure 8c). The
29 underestimation of the simulated CO_2 concentration must mainly result from the
30 representation errors in the atmospheric transport due to the coarser model resolution.



1 For Palos Verdes, however, none of the model results match the observations. All of the
2 runs show a peak in the simulated CO₂ concentration around 0800 PST, which very likely
3 corresponds to the eastward marine flow as a part of the Catalina eddy (e.g., Bosart,
4 1983; Davis et al., 2000). This CO₂ concentration peak is incorrectly reproduced by the
5 model advecting the FFCO₂ emitted from the strong point sources in Long Beach,
6 California (Figure 1d) and in turn contaminating the air of Palos Verdes.

7

8 **4 Spatial pattern of the surface CO₂**

9 The spatial pattern of surface CO₂ concentration exhibits diurnal variability over the LA
10 megacity due to the complexity of the topography and the variability of circulation
11 patterns, PBL heights, and FFCO₂ emissions. Each plays an important role in sequence or
12 at the same time. Here, we only focus on the pattern at 1400 PST when the atmospheric
13 CO₂ concentration is well mixed in the PBL. At 1400 PST, there is a close relationship
14 between CO₂ concentration and atmospheric transport; the error due to the PBL height
15 determination is at a minimum. For the same reason, we show that FFCO₂ emissions do
16 not play a dominant role around 1400 PST unless there are strong local signals from point
17 sources, such as power plants, refineries, airports etc.

18 In this section, we define the 1.3-km WRF-Hestia run as the reference simulation. For
19 simplicity, all of the relevant CO₂ spatial patterns we present are selected from the second
20 model layer (about 24 m AGL). Figure 9a and 9b display the topography and the average
21 CO₂ concentration at 1400 PST overlaid with the first empirical orthogonal function
22 (EOF1) of the surface wind pattern, respectively. The locations of the 13 GHG
23 measurement sites in the LA megacity domain are marked in the figures (see Table 3 and
24 Figure S1 for details about the observation sites). Note that The 2015-era surface GHG
25 measurement network includes 14 sites in total, while 13 sites are included in the
26 innermost model domain. According to the geography mentioned in section 2.1, the
27 Granada Hills (GH), Compton, USC, and sites are located in the West Coast Basin, the
28 Pasadena and Mt. Wilson (MWO) sites are in the Central Basin, and California State
29 University Fullerton (CSUF), Ontario, and San Bernardino (SB) sites are in the Orange
30 County Coastal Plan. Additionally, the Dryden and Victorville (VV) sites are located in



1 deserts; the Palos Verdes (PV), University of California Irvine (UCI), and San Clemente
2 Island (SCI) are on the coast. Although the Dryden site is actually a TCCON site, in the
3 analysis, we assume it is a near-surface point measurement like other sites for simplicity.

4 Blocked by the mountains, the emitted CO₂ is trapped in the basin; the desert is as clean
5 as the upwind ocean. Specifically, Dryden (not shown on the figure), VV, SCI (not
6 shown on the figure), Palos Verdes and UCI are much cleaner than other sites (Figure
7 9b). At 1400 PST, sea breeze prevails over the LA megacity. Affected by the geometry of
8 Palos Verdes Peninsula, the sea breeze is divided into west and southwest onshore flows
9 and then converge in the Central Basin. Strong CO₂ signals emitted from electricity
10 production and industry (with annual emission of 86.9 million kgC, Figure 1d) are
11 trapped in a limited area. We notice that the south-western flow, which appears stronger
12 than the western flow, prevents the high CO₂ concentration in the West Coast Basin from
13 propagating further east and dilutes into the Central Basin. Controlled by the orography,
14 strong southerly flows occur between the Santa Monica and San Gabriel Mountains,
15 keeping the contaminated air from propagating to the west. Driven by the same
16 meteorology, the 1.3-km WRF-Vulcan run shows a more smeared out CO₂ concentration
17 over the LA megacity (Figure 9c) due to the coarser resolution of the original Vulcan
18 emissions. High CO₂ plumes seen in the 1.3-km WRF-Hestia run from point sources are
19 replaced by wide area of the elevated CO₂ concentration in the 1.3-km WRF-Vulcan. The
20 large differences in the simulated surface CO₂ fields between the 1.3-km WRF-Hestia and
21 WRF-Vulcan runs are around LAX and north of the Palos Verdes Peninsula where strong
22 point sources are located (dipole-like pattern in Figure 9d).

23

24 **5 Sampling density of the 2015-era GHG measurement network**

25 In this section, we present a forward network design framework, using the modelled CO₂
26 concentrations and their relationship with neighbouring grid cells. Compared to previous
27 studies using tower footprints (i.e. linearized adjoint models) as Kort et al. (2013), we
28 propose here a forward model assessment of the network using our high-resolution WRF
29 results. We assume that each observation site can be associated with a specific CO₂ air
30 mass at any given time. To define this CO₂ air mass, we estimate the spatial coherence in



1 the modelled CO₂ concentration fields. We constrain the coverage of each LA GHG
2 measurement site by calculating the simultaneous correlation of the site to the rest of the
3 domain using the simulated CO₂ concentration time series. Figure 10 shows the
4 correlation map (R) of each site for the 1.3-km WRF-Hestia run. Only areas meeting a
5 significance level of 0.01 in the t-test ($|R| \geq 0.46$) are coloured. Based on the spatial
6 patterns of the correlation maps, all of the observation sites can be grouped into (i)
7 coastal/island sites, i.e., UCI, SCI, and Palos Verdes (right three panels in bottom row of
8 Figure 10), (ii) western basin sites, i.e., GH, Pasadena, MWO, USC, and Compton (top
9 row in Figure 10), (iii) eastern basin sites, (i.e., CSUF, Ontario, SB; middle row in Figure
10 10), and (iv) desert sites, i.e., Dryden and VV (left two panels in bottom row of Figure
11 10).

12 Not surprisingly, the coastal/island sites are mainly correlated with CO₂ concentration in
13 upwind areas offshore where there is limited FFCO₂ contamination. The white channel
14 from Catalina Island to the Huntington Beach area demonstrates the influence of terrain-
15 induced flows and mountain blocking. The western basin sites are mainly correlated with
16 CO₂ concentration throughout the western portion of the basin, and the eastern basin sites
17 are mainly correlated with CO₂ concentration throughout the eastern portion of the basin.
18 The desert sites are anti-correlated with the basin. CSUF also shows anti-correlation with
19 the desert. Two reasons can explain this anti-correlation. Firstly, CO₂ is trapped and
20 accumulates in the basin due to the mountain barrier. Secondly, after CO₂ accumulates in
21 the basin over a certain amount of time, episodic strong sea breezes may push this basin
22 CO₂ over the mountains to the desert. As a result, the basin will be relatively clean while
23 the desert is contaminated.

24 Based on the correlation maps, we can also see how the coverage of each site varies with
25 the FFCO₂ emissions data products and with the WRF model resolutions. Figure 11
26 shows the correlation maps across the runs for the Compton, Palos Verdes, and CSUF
27 stations. All runs use the optimal physics we determined for the LA megacity, i.e.,
28 MYNN_UCM. The correlation maps for each site differ with the FFCO₂ emissions data
29 product used, model resolution, or their combination (Figure 11). Given that the 1.3-km
30 WRF-Hestia is the reference run, the difference of this to the 1.3-km WRF-Vulcan run
31 reflects the errors induced by emissions resolution. The difference between the 4-km



1 WRF-Hestia run and the 1.3-km WRF-Hestia run reflects by the model representation
2 errors. The 4-km WRF-Vulcan run is subject to model representation errors and emission
3 aggregation errors at the same time. For simplicity, we will not emphasize but show the
4 comparison of the 4-km WRF-Vulcan to the others.

5 Compton is isolated from the rest of the basin in the 1.3-km WRF-Hestia run but
6 correlated with most of the basin in the 1.3-km WRF-Vulcan run. A similar discrepancy
7 is seen for Palos Verdes. Additionally, Palos Verdes appears to be a clean site in the 1.3-
8 km WRF-Hestia run but dramatically contaminated in the 1.3-km WRF-Vulcan run (even
9 correlated with the LA downtown area). For CSUF, the anti-correlation between basin
10 and desert noted above is not visible in the 1.3-km WRF-Vulcan run. Compared to the
11 1.3-km WRF-Hestia run, the 4-km WRF-Hestia run overall shows a somewhat larger
12 region with significant correlation for each site.

13 To highlight the discrepancy of the spatial pattern caused by the model representation
14 errors and emission aggregation errors in the view of the existing GHG measurement
15 network, a composite map for each run is shown in Figure 12. These maps are
16 constructed by determining the number of sites for which the absolute value of R is
17 greater than 0.46 for each grid cell (i.e., colour-filled area in Figure 10 and 11). $R=0.46$ is
18 the critical value for the t -test at the significance level of 0.01. In the 1.3-km WRF-Hestia
19 run (reference), the West Coastal Basin and Orange County Coastal Plain are correlated
20 with up to 6 measurement sites. A gap appears over the Central Basin correlated with up
21 to 3 sites due to the wind pattern (Figure 9a and 9b). The San Gabriel Mountains and
22 Peninsular Ranges are rarely correlated to any of the sites due to the elevated terrain. The
23 4-km WRF-Hestia run shows a similar pattern but with more sites covered over the
24 Peninsular Ranges and the coast because of the failure to resolve topography by the 4-km
25 model resolution.

26 In the 1.3-km WRF-Vulcan run, by contrast, a large area of the basin is correlated with
27 most of the sites (9 sites out of 13). The Compton area is even correlated with 11 sites,
28 which is only correlated with about two sites in the 1.3-km WRF-Hestia run. A similar
29 contrast can be seen for the GH, USC, and Palos Verdes areas where the multiple strong
30 point sources nearby in Hestia-LA have been aggregated into one 10 km by 10 km grid



1 cell in Vulcan (Figure 1d vs.1c). Relatively coarser FFCO₂ emissions artificially increase
2 the coverage of each site, which highlights the importance of using Hestia for the CO₂
3 simulation for urban environment to represent the spatial variability in CO₂ and design
4 the optimal network of surface GHG measurement.

5

6 **6 Discussion**

7 Isotopic tracer radiocarbon (¹⁴C) can be used for distinguishing between fossil fuel and
8 biogenic sources of CO₂ (Djuricin et al., 2010; Newman et al., 2013; Newman et al.,
9 2008; Pataki et al., 2006; Pataki et al., 2007; Levin et al., 2003; Miller et al., 2012;
10 Turnbull et al., 2006; Turnbull et al., 2009). During CalNex-LA, two-weeks' flask
11 samples were combined to produce two CO₂ samples for extracting anthropogenic and
12 biogenic signals from the total CO₂ concentration. Note that the two samples for Palos
13 Verdes were sampled from 1 May to 31 May and from 1 June to 30 June, not exactly
14 overlapping the CalNex-LA period; the two for Pasadena were sampled from 15 May to
15 31 May and from 1 June to 15 June, overlapping the CalNex-LA period. See Newman et
16 al. (2015) for details about the sites and sampling information. Figure 13 presents the
17 comparisons of the modelled and flask-sampled anthropogenic fossil fuel and biogenic
18 CO₂. From both the flask samples and model simulations, the CO₂ signal from the
19 biosphere is much weaker than FFCO₂ in the LA megacity. The two-week flask sampled
20 biogenic CO₂ is about 2 ppm on average. We notice that the 1.3-km WRF-Vulcan
21 overestimates the FFCO₂ concentrations about 20 ppm over the second half of the month
22 (Figure 13d), implying that low-resolution CO₂ emissions can be very critical for a coast
23 site (complex terrain) with strong point source nearby.

24 Strong temporal variability of the simulated biogenic and FFCO₂ can be seen for both
25 sites (Figure 13a,13c,13e,13g). For the Pasadena site, the 1.3-km run shows nearly flat
26 biogenic CO₂ concentrations during 15 May to 30 May when the 4-km run has more
27 variability (Figure 13e). We notice that a large botanical garden covering 207 acres (i.e.
28 The Huntington Library) is about 1.6 km away from the Pasadena site, which may
29 suggest that higher model resolution (1.3 km vs. 4 km) could be impacted by a change in
30 land cover. However, there is still up to about 3-ppm discrepancy in the modelled



1 biogenic CO₂ from the flask samples (Figure 13f). Similar discrepancy can be seen for
2 Palos Verdes as well (Figure 13h). Reasonably determining CO₂ from biogenic sources
3 remains challenging. Additional measurements are needed to constrain biogenic fluxes.
4 Here, we focus on FFCO₂ emissions that dominate local CO₂ signals across the basin.

5 The results presented in this paper have shown that the choice of model resolution and
6 emission products can strongly influence the interpretation of atmospheric CO₂ signals.
7 Hestia quantifies FFCO₂ emissions down to individual buildings and roadways, in which
8 strong point sources create large plumes that are extremely sensitive to atmospheric
9 transport. Reproducing dynamics realistically by the atmospheric transport model is
10 crucial around strong point sources, such as power plants, refineries, airports, etc. For
11 instance, a considerable number of point sources are located in Long Beach (harbours,
12 Figure 1d), about 7 km away from Palos Verdes. In late spring and summer, Palos Verdes
13 is a clean site, with little evidence of FFCO₂ emissions from the LA megacity most of the
14 time. However, we can clearly see oftentimes Palos Verdes is simulated to be
15 contaminated by FFCO₂ in all of the runs, especially during early morning (Figure 8b)
16 due to incorrectly simulated east marine flows advecting the strong FFCO₂ emissions,
17 which cannot be seen in the observations. Bias in wind speed and direction becomes
18 critical for such a location. Palos Verdes may be challenging for the atmospheric model if
19 used as a background site.

20 For a location like Compton with strong point sources nearby emitting CO₂ at 86.9
21 million kgC per year (recorded in Hestia-LA version 1.0), a fine resolution emission
22 product becomes very important due to the strong FFCO₂ gradient. A relatively coarse
23 emission product likely produces a spurious signal due to aggregating a strong point
24 source into a large grid cell (Figure 9b and 9c). For instance, dipole-like CO₂ gradients
25 were created in the difference between the 1.3-km WRF-Vulcan and WRF-Hestia runs
26 (Figure 9d).

27 In this paper, we focus on the spatial distribution of the CO₂ concentration over the LA
28 megacity. The choice of model resolution also significantly impacts the vertical gradients
29 of the CO₂ concentration as a result of the terrain resolved. The 1.3-km model runs
30 approximates the elevation of MWO as 1129 m, while the 4 km runs is 753 m; the actual



1 elevation is 1600 m. The representation errors in the 4-km model resolution are relatively
2 large. When there is better topographic resolution, more CO₂ is accumulated in the basin
3 due to blocking by the mountains. Around noon, the model results show CO₂
4 enhancement of 10 ppm over MWO in both of the 1.3-km WRF-Vulcan and WRF-Hestia
5 runs but only up to 3 ppm in the 4-km model runs. Additionally, because of the reasons
6 above, reasonable sampling strategy is worth investigating for the mountain sites like
7 MWO (e.g., Law et al., 2008). Similar problems exist for a site like Palos Verdes, since
8 the coastline resolved varies with the model resolutions, as does the topography. Model
9 sampling strategy is therefore recommended even at 1.3-km resolution, as no clear
10 improvement in the meteorological evaluation was observed in horizontal.

11 Figure 10 presents the simultaneous correlation maps for each site in terms of the
12 simulated CO₂ concentration time series. The coverage of the correlation maps is
13 determined by two factors at the same time: atmospheric transport and surface fluxes.
14 This method differs from the footprint method (Kort et al., 2013). The footprint method
15 indicates the influence of the atmospheric transport to the location of the observation
16 only; no emission pattern was considered. Here both transport and emissions play a role
17 in the area covered by the observation site. Therefore, the correlation maps are subject to
18 overestimation of the influence area versus the footprint method, due to the complicated
19 nature of the atmospheric integrator. As an example, in Figure 10, the coloured grids of
20 the correlation map are not necessarily *physically* related to the observation site. Those
21 far from the site may lose the track of the initial sources. Conversely, there is definitely
22 no *physical* influence from the uncorrelated areas to the observation site. Figure 14 shows
23 the fraction of the total FFCO₂ emissions over the LA megacity as function of the number
24 of the observation sites for all of the runs. Because of the reason above, we focus on the
25 uncorrelated areas only. Assuming that the coverage of the GHG measurement network is
26 not sufficient if an area is correlated to less than or equal to two sites, then ~28.9 % of
27 FFCO₂ is potentially under-constrained by the current GHG measurement sites (Figure
28 14a: WRF-Hestia 1.3-km). These areas include most of the mountains, Santa Monica Bay
29 and the upwind coast, and the south part of the Central Basin (Figure 11), about 21.1 %
30 of total area. However, this analysis is a qualitative assessment of the observational



1 constraint. Consideration of errors in the CO₂ emissions needs to be taken into account
2 for a complete assessment of the network.

3 Figure 14 also reflects the impact of the FFCO₂ emissions used to simulate the CO₂ fields.
4 In the 1.3-km WRF-Hestia run, there are no areas covered by more than six sites, while
5 the 1.3-km WRF-Vulcan run shows 39.8 % of FFCO₂ emissions over the LA megacity to
6 be covered by more than six sites. Additionally, the distribution appears nearly normal
7 for the 1.3-km WRF-Vulcan run. A similar discrepancy is seen between the 4-km WRF-
8 Hestia and WRF-Vulcan runs. These differences between the WRF-Hestia and WRF-
9 Vulcan runs further highlight the importance of using the high-resolution FFCO₂
10 emissions product for the urban CO₂ simulation.

11

12 **7 Conclusion**

13 A set of WRF configurations varying by PBL scheme, urban surface scheme, and model
14 resolution has been evaluated by comparing the PBL height determined by aircraft
15 profiles and ceilometer, wind speed and wind direction measured by radar wind profiler,
16 and surface atmospheric states measured by NWS stations. The results suggest that, there
17 is no remarkable difference between the 4-km and 1.3-km resolution simulations in terms
18 of atmospheric model performances in horizontal, but the 1.3-km model runs resolve the
19 vertical gradients of wind fields and PBL height somewhat better as demonstrated. The
20 model inter-comparisons show the model using MYNN_UCM has overall better
21 performance than others. Coupled to FFCO₂ emissions products (Hestia-LA and Vulcan
22 2.2), a land-atmosphere modelling system was built with MYNN_UCM for studying the
23 heterogeneity of urban CO₂ emissions over the LA megacity.

24 The Vulcan and Hestia-LA FFCO₂ emission products were used to investigate the impact
25 of the model representation errors and emission aggregation errors on the modelled CO₂
26 concentration. Compared to the in-situ measurements during CalNex-LA, the 1.3-km
27 modelled CO₂ concentrations clearly outperform the results at 4-km resolution for
28 capturing both the spatial distribution and the temporal variability of the urban CO₂
29 signals due to strong FFCO₂ emission gradients across the LA megacity, even though no
30 clear improvement in the meteorological evaluation was observed across the basin. The



1 inter-comparison of the WRF-Hestia and WRF-Vulcan runs reinforces the importance of
2 using high-resolution emission products to represent correct, large spatial gradients in
3 atmospheric CO₂ concentrations for urban environments.

4 Based on the 1.3-km WRF-Hestia run, the coverage of the current GHG measurement
5 site over the LA megacity was evaluated using the modelled spatial correlations. Kort et
6 al. (2013) concluded a network of eight surface observation sites provided the minimum
7 sampling required for accurate monitoring of FFCO₂ emissions in LA using Vulcan at 4-
8 km model resolution. In this study, however, using Vulcan FFCO₂ emissions tend to
9 overestimate the observational constraint spatially, suggesting that the information lies in
10 multiple fine-scale plumes rather than a single urban dome over the Los Angeles basin.
11 Thanks to the much finer-resolution model and FFCO₂ emission product Hestia-LA, the
12 coverage of each observation site seems constrained to a more limited area. Using a high-
13 resolution emission data product and a high-resolution model configuration is necessary
14 for accurately assessing the urban measurement network.

15

16 **8 Author contributions**

17 S. Feng and T. Lauvaux designed the model experiments, evaluated the model
18 performance, and developed the assessment of the measuring network; S. Newman
19 provided the calibrated CO₂ measurements and the support for the model evaluations. P.
20 Rao, R. Patarasuk, D. O’Keeffe, J. Huang, Y. Song, K.R. Gurney developed and prepared
21 the Vulcan and Hestia emission products; R. Ahmadov contributed to the developments
22 of the WRF-VPRM model and relevant guideline; A. Deng provided quality control to
23 the observations from the National Weather Stations; L.I. Díaz-Isaac tested PBL
24 algorithms; S. Jeong and M.L. Fischer provided the background CO₂ concentration for
25 the LA megacity (region); R.M. Duren, C. Gerbig, Z. Li, C. E. Miller, S. Sander, K.W.
26 Wong, and Y. Yung provided comments and discussed the results of the study.

27

28 **Acknowledgements**



1 A portion of this work was performed at the Jet Propulsion Laboratory, California
2 Institute of Technology, under contract with NASA. The Megacities Carbon Project is
3 sponsored in part by the National Institute of Standards and Technology (NIST). S.
4 Newman acknowledges funding from the Caltech/JPL President & Director's Research
5 and Development Fund. K. R. Gurney thanks NIST grant 70NANB14H321.R.
6 Ahmadov was supported by the US Weather Research Program within the NOAA/OAR
7 Office of Weather and Air Quality. S. Jeong and M.L. Fischer acknowledge the support
8 by the Laboratory Directed Research and Development Program, Office of Science, of
9 the US Department of Energy under Contract No. DE-AC02-05CH11231. Thanks to W.
10 Angevine at NOAA for radar wind profiler data, K. Aikin at NOAA for Aircraft WP-3D
11 data, and B. Lefer at University of Houston for ceilometer data.



1 **References**

- 2 Ahmadov, R., Gerbig, C., Kretschmer, R., Koerner, S., Neininger, B., Dolman, A. J., and
3 Sarrat, C.: Mesoscale covariance of transport and CO₂ fluxes: Evidence from
4 observations and simulations using the WRF-VPRM coupled atmosphere-biosphere
5 model, *Journal of Geophysical Research: Atmospheres*, 112, D22107,
6 10.1029/2007JD008552, 2007.
- 7 Ahmadov, R., Gerbig, C., Kretschmer, R., Körner, S., Rödenbeck, C., Bousquet, P., and
8 Ramonet, M.: Comparing high resolution WRF-VPRM simulations and two global CO₂
9 transport models with coastal tower measurements of CO₂, *Biogeosciences*, 6, 807-817,
10 10.5194/bg-6-807-2009, 2009.
- 11 Angevine, W. M., Eddington, L., Durkee, K., Fairall, C., Bianco, L., and Brioude, J.:
12 Meteorological Model Evaluation for CalNex 2010, *Monthly Weather Review*, 140,
13 3885-3906, 10.1175/MWR-D-12-00042.1, 2012.
- 14 Asefi-Najafabady, S., Rayner, P. J., Gurney, K. R., McRobert, A., Song, Y., Coltin, K.,
15 Huang, J., Elvidge, C., and Baugh, K.: A multiyear, global gridded fossil fuel CO₂
16 emission data product: Evaluation and analysis of results, *Journal of Geophysical*
17 *Research: Atmospheres*, 119, 10,213-210,231, 10.1002/2013JD021296, 2014.
- 18 Baker, D. F., Law, R. M., Gurney, K. R., Rayner, P., Peylin, P., Denning, A. S.,
19 Bousquet, P., Bruhwiler, L., Chen, Y. H., Ciais, P., Fung, I. Y., Heimann, M., John, J.,
20 Maki, T., Maksyutov, S., Masarie, K., Prather, M., Pak, B., Taguchi, S., and Zhu, Z.:
21 TransCom 3 inversion intercomparison: Impact of transport model errors on the
22 interannual variability of regional CO₂ fluxes, 1988–2003, *Global Biogeochemical*
23 *Cycles*, 20, n/a-n/a, 10.1029/2004GB002439, 2006.
- 24 Baker, K. R., Misener, C., Obland, M. D., Ferrare, R. A., Scarino, A. J., and Kelly, J. T.:
25 Evaluation of surface and upper air fine scale WRF meteorological modeling of the May
26 and June 2010 CalNex period in California, *Atmospheric Environment*, 80, 299-309,
27 <http://dx.doi.org/10.1016/j.atmosenv.2013.08.006>, 2013.
- 28 Bosart, L. F.: Analysis of a California Catalina Eddy Event, *Monthly Weather Review*,
29 111, 1619-1633, 10.1175/1520-0493(1983)111<1619:AOACCE>2.0.CO;2, 1983.



- 1 Bougeault, P., and Lacarrere, P.: Parameterization of Orography-Induced Turbulence in a
2 Mesobeta-Scale Model, *Monthly Weather Review*, 117, 1872-1890, 10.1175/1520-
3 0493(1989)117<1872:POOITI>2.0.CO;2, 1989.
- 4 Bréon, F. M., Broquet, G., Puygrenier, V., Chevallier, F., Xueref-Remy, I., Ramonet, M.,
5 Dieudonné, E., Lopez, M., Schmidt, M., Perrussel, O., and Ciais, P.: An attempt at
6 estimating Paris area CO₂ emissions from atmospheric concentration measurements,
7 *Atmos. Chem. Phys.*, 15, 1707-1724, 10.5194/acp-15-1707-2015, 2015.
- 8 Brioude, J., Angevine, W. M., Ahmadov, R., Kim, S. W., Evan, S., McKeen, S. A., Hsie,
9 E. Y., Frost, G. J., Neuman, J. A., Pollack, I. B., Peischl, J., Ryerson, T. B., Holloway, J.,
10 Brown, S. S., Nowak, J. B., Roberts, J. M., Wofsy, S. C., Santoni, G. W., Oda, T., and
11 Trainer, M.: Top-down estimate of surface flux in the Los Angeles Basin using a
12 mesoscale inverse modeling technique: assessing anthropogenic emissions of CO, NO_x
13 and CO₂ and their impacts, *Atmos. Chem. Phys.*, 13, 3661-3677, 10.5194/acp-13-3661-
14 2013, 2013.
- 15 C40: Climate 40 Group, <http://live.c40cities.org/>, 2012.
- 16 Chen, D., Li, Q., Stutz, J., Mao, Y., Zhang, L., Pikelnaya, O., Tsai, J. Y., Haman, C.,
17 Lefer, B., Rappenglück, B., Alvarez, S. L., Neuman, J. A., Flynn, J., Roberts, J. M.,
18 Nowak, J. B., de Gouw, J., Holloway, J., Wagner, N. L., Veres, P., Brown, S. S.,
19 Ryerson, T. B., Warneke, C., and Pollack, I. B.: WRF-Chem simulation of NO_x and O₃
20 in the L.A. basin during CalNex-2010, *Atmospheric Environment*, 81, 421-432,
21 <http://dx.doi.org/10.1016/j.atmosenv.2013.08.064>, 2013.
- 22 Chen, F., and Dudhia, J.: Coupling an Advanced Land Surface-Hydrology Model with
23 the Penn State-NCAR MM5 Modeling System. Part I: Model Implementation and
24 Sensitivity, *Monthly Weather Review*, 129, 569-585, 10.1175/1520-
25 0493(2001)129<0569:CAALSH>2.0.CO;2, 2001.
- 26 Conil, S., and Hall, A.: Local Regimes of Atmospheric Variability: A Case Study of
27 Southern California, *Journal of Climate*, 19, 4308-4325, 10.1175/JCLI3837.1, 2006.
- 28 Davis, C., Low-Nam, S., and Mass, C.: Dynamics of a Catalina Eddy Revealed by
29 Numerical Simulation, *Monthly Weather Review*, 128, 2885-2904, 10.1175/1520-



- 1 0493(2000)128<2885:DOACER>2.0.CO;2, 2000.
- 2 Deng, A., Stauffer, D. R., Gaudet, B. J., Dudhia, J., Hacker, J., Bruyere, C., Wu, W.,
3 Vandenberghe, F., Liu, Y., and Bourgeois, A.: Update on WRF-ARW End-to-End Multi-
4 scale FDDA System, 10th Annual WRF Users' Workshop, Boulder, CO, June 23, 2009.
- 5 Díaz Isaac, L. I., Lauvaux, T., Davis, K. J., Miles, N. L., Richardson, S. J., Jacobson, A.
6 R., and Andrews, A. E.: Model-data comparison of MCI field campaign atmospheric
7 CO₂ mole fractions, *Journal of Geophysical Research: Atmospheres*, 119,
8 2014JD021593, 10.1002/2014JD021593, 2014.
- 9 Djuricin, S., Pataki, D. E., and Xu, X.: A comparison of tracer methods for quantifying
10 CO₂ sources in an urban region, *Journal of Geophysical Research: Atmospheres*, 115,
11 n/a-n/a, 10.1029/2009JD012236, 2010.
- 12 Engelen, R. J., Denning, A. S., and Gurney, K. R.: On error estimation in atmospheric
13 CO₂ inversions, *Journal of Geophysical Research: Atmospheres*, 107, 4635,
14 10.1029/2002JD002195, 2002.
- 15 Enting, I. G., Heimann, M., Wigley, T. M. L., Commonwealth, S., and Industrial
16 Research, O.: Future emissions and concentrations of carbon dioxide: key
17 ocean/atmosphere/land analyses, Division of Atmospheric Research technical paper ;no.
18 31, 120 p., CSIRO, Australia, 120 p. pp., 1994.
- 19 Etheridge, D. M., Steele, L. P., Langenfelds, R. L., Francey, R. J., Barnola, J. M., and
20 Morgan, V. I.: Natural and anthropogenic changes in atmospheric CO₂ over the last 1000
21 years from air in Antarctic ice and firn, *Journal of Geophysical Research: Atmospheres*,
22 101, 4115-4128, 10.1029/95JD03410, 1996.
- 23 Gerbig, C., Körner, S., and Lin, J. C.: Vertical mixing in atmospheric tracer transport
24 models: error characterization and propagation, *Atmos. Chem. Phys.*, 8, 591-602,
25 10.5194/acp-8-591-2008, 2008.
- 26 Grell, G. A., and Dévényi, D.: A generalized approach to parameterizing convection
27 combining ensemble and data assimilation techniques, *Geophysical Research Letters*, 29,
28 38-31-38-34, 10.1029/2002GL015311, 2002.
- 29 Gurney, K. R., Law, R. M., Denning, A. S., Rayner, P. J., Baker, D., Bousquet, P.,



- 1 Bruhwiler, L., Chen, Y.-H., Ciais, P., Fan, S., Fung, I. Y., Gloor, M., Heimann, M.,
2 Higuchi, K., John, J., Maki, T., Maksyutov, S., Masarie, K., Peylin, P., Prather, M., Pak,
3 B. C., Randerson, J., Sarmiento, J., Taguchi, S., Takahashi, T., and Yuen, C.-W.:
4 Towards robust regional estimates of CO₂ sources and sinks using atmospheric transport
5 models, *Nature*, 415, 626-630,
6 http://www.nature.com/nature/journal/v415/n6872/supinfo/415626a_S1.html, 2002.
- 7 Gurney, K. R., Mendoza, D. L., Zhou, Y., Fischer, M. L., Miller, C. C., Geethakumar, S.,
8 and de la Rue du Can, S.: High Resolution Fossil Fuel Combustion CO₂ Emission Fluxes
9 for the United States, *Environmental Science & Technology*, 43, 5535-5541,
10 10.1021/es900806c, 2009.
- 11 Gurney, K. R., Razlivanov, I., Song, Y., Zhou, Y., Benes, B., and Abdul-Massih, M.:
12 Quantification of Fossil Fuel CO₂ Emissions on the Building/Street Scale for a Large
13 U.S. City, *Environmental Science & Technology*, 46, 12194-12202, 10.1021/es3011282,
14 2012.
- 15 Gurney, K. R., Romero-Lankao, P., Seto, K. C., Hutyra, L. R., Duren, R., Kennedy, C.,
16 Grimm, N. B., Ehleringer, J. R., Marcutuillio, P., Hughes, S., Pincetl, S., Chester, M. V.,
17 Runfola, D. M., Feddema, J. J., and Sperling, J.: Climate change: Track urban emissions
18 on a human scale citation, *Nature*, 525, 179–181, 10.1038/525179a, 2015.
- 19 Haman, C. L., Lefer, B., and Morris, G. A.: Seasonal Variability in the Diurnal Evolution
20 of the Boundary Layer in a Near-Coastal Urban Environment, *Journal of Atmospheric
21 and Oceanic Technology*, 29, 697-710, 10.1175/JTECH-D-11-00114.1, 2012.
- 22 Hong, S.-Y., Dudhia, J., and Chen, S.-H.: A Revised Approach to Ice Microphysical
23 Processes for the Bulk Parameterization of Clouds and Precipitation, *Monthly Weather
24 Review*, 132, 103-120, 10.1175/1520-0493(2004)132<0103:ARATIM>2.0.CO;2, 2004.
- 25 Hong, S.-Y., Noh, Y., and Dudhia, J.: A New Vertical Diffusion Package with an Explicit
26 Treatment of Entrainment Processes, *Monthly Weather Review*, 134, 2318-2341,
27 10.1175/MWR3199.1, 2006.
- 28 Houghton, R. A.: The annual net flux of carbon to the atmosphere from changes in land
29 use 1850–1990*, *Tellus B*, 51, 298-313, 10.1034/j.1600-0889.1999.00013.x, 1999.



- 1 Iacono, M. J., Delamere, J. S., Mlawer, E. J., Shephard, M. W., Clough, S. A., and
2 Collins, W. D.: Radiative forcing by long-lived greenhouse gases: Calculations with the
3 AER radiative transfer models, *Journal of Geophysical Research: Atmospheres*, 113, n/a-
4 n/a, 10.1029/2008JD009944, 2008.
- 5 IPCC: Climate Change 2013. The Physical Science Basis. Contribution of Working
6 Group I to the Fifth Assessment Report of the Intergovernmental Panel on Climate
7 Change [Stocker, T.F., D. Qin, G.-K. Plattner, M. Tignor, S.K. Allen, J. Boschung, A.
8 Nauels, Y. Xia, V. Bex and P.M. Midgley (eds.)], Cambridge University Press,
9 Cambridge, United Kingdom and New York, NY, USA, 1535pp., 2013.
- 10 Jacob, D. J., Crawford, J. H., Maring, H., Clarke, A. D., Dibb, J. E., Emmons, L. K.,
11 Ferrare, R. A., Hostetler, C. A., Russell, P. B., Singh, H. B., Thompson, A. M., Shaw, G.
12 E., McCauley, E., Pederson, J. R., and Fisher, J. A.: The Arctic Research of the
13 Composition of the Troposphere from Aircraft and Satellites (ARCTAS) mission: design,
14 execution, and first results, *Atmos. Chem. Phys.*, 10, 5191-5212, 10.5194/acp-10-5191-
15 2010, 2010.
- 16 Janjić, Z. I.: The Step-Mountain Eta Coordinate Model: Further Developments of the
17 Convection, Viscous Sublayer, and Turbulence Closure Schemes, *Monthly Weather*
18 *Review*, 122, 927-945, 10.1175/1520-0493(1994)122<0927:TSMECM>2.0.CO;2, 1994.
- 19 Jeong, S., Hsu, Y.-K., Andrews, A. E., Bianco, L., Vaca, P., Wilczak, J. M., and Fischer,
20 M. L.: A multitower measurement network estimate of California's methane emissions,
21 *Journal of Geophysical Research: Atmospheres*, 118, 11,339-311,351,
22 10.1002/jgrd.50854, 2013.
- 23 Kort, E. A., Frankenberg, C., Miller, C. E., and Oda, T.: Space-based observations of
24 megacity carbon dioxide, *Geophysical Research Letters*, 39, L17806,
25 10.1029/2012GL052738, 2012.
- 26 Kort, E. A., Angevine, W. M., Duren, R., and Miller, C. E.: Surface observations for
27 monitoring urban fossil fuel CO₂ emissions: Minimum site location requirements for the
28 Los Angeles megacity, *Journal of Geophysical Research: Atmospheres*, 118, 1577-1584,
29 10.1002/jgrd.50135, 2013.



- 1 Kretschmer, R., Gerbig, C., Karstens, U., and Koch, F. T.: Error characterization of CO₂
2 vertical mixing in the atmospheric transport model WRF-VPRM, *Atmos. Chem. Phys.*,
3 12, 2441-2458, 10.5194/acp-12-2441-2012, 2012.
- 4 Kretschmer, R., Gerbig, C., Karstens, U., Biavati, G., Vermeulen, A., Vogel, F.,
5 Hammer, S., and Totsche, K. U.: Impact of optimized mixing heights on simulated
6 regional atmospheric transport of CO₂, *Atmos. Chem. Phys.*, 14, 7149-7172,
7 10.5194/acp-14-7149-2014, 2014.
- 8 Kusaka, H., Kondo, H., Kikegawa, Y., and Kimura, F.: A Simple Single-Layer Urban
9 Canopy Model For Atmospheric Models: Comparison With Multi-Layer And Slab
10 Models, *Boundary-Layer Meteorol.*, 101, 329-358, 10.1023/A:1019207923078, 2001.
- 11 Kusaka, H., and Kimura, F.: Thermal Effects of Urban Canyon Structure on the
12 Nocturnal Heat Island: Numerical Experiment Using a Mesoscale Model Coupled with
13 an Urban Canopy Model, *Journal of Applied Meteorology*, 43, 1899-1910,
14 10.1175/JAM2169.1, 2004a.
- 15 Kusaka, H., and Kimura, F.: Coupling a Single-Layer Urban Canopy Model with a
16 Simple Atmospheric Model: Impact on Urban Heat Island Simulation for an Idealized
17 Case, *Journal of the Meteorological Society of Japan. Ser. II*, 82, 67-80,
18 10.2151/jmsj.82.67, 2004b.
- 19 Lac, C., Donnelly, R. P., Masson, V., Pal, S., Riette, S., Donier, S., Queguiner, S.,
20 Tanguy, G., Ammoura, L., and Xueref-Remy, I.: CO₂ dispersion modelling over Paris
21 region within the CO₂-MEGAPARIS project, *Atmos. Chem. Phys.*, 13, 4941-4961,
22 10.5194/acp-13-4941-2013, 2013.
- 23 Lauvaux, T., Uliasz, M., Sarrat, C., Chevallier, F., Bousquet, P., Lac, C., Davis, K. J.,
24 Ciais, P., Denning, A. S., and Rayner, P. J.: Mesoscale inversion: first results from the
25 CERES campaign with synthetic data, *Atmos. Chem. Phys.*, 8, 3459-3471, 10.5194/acp-
26 8-3459-2008, 2008.
- 27 Lauvaux, T., Pannekoucke, O., Sarrat, C., Chevallier, F., Ciais, P., Noilhan, J., and
28 Rayner, P. J.: Structure of the transport uncertainty in mesoscale inversions of CO₂
29 sources and sinks using ensemble model simulations, *Biogeosciences*, 6, 1089-1102,



- 1 10.5194/bg-6-1089-2009, 2009.
- 2 Lauvaux, T., Schuh, A. E., Bocquet, M., Wu, L., Richardson, S., Miles, N., and Davis, K.
3 J.: Network design for mesoscale inversions of CO₂ sources and sinks, 2012, 64,
4 10.3402/tellusb.v64i0.17980, 2012.
- 5 Lauvaux, T., Miles, N. L., Deng, A., Richardson, S. J., Cambaliza, M. O., Davis, K. J.,
6 Gaudet, B., Gurney, K. R., Huang, J., Karion, A., Oda, T., Patarasuk, R., Razlivanov, I.,
7 Sarmiento, D., Shepson, P. B., Sweeney, C., Turnbull, J. C., and Wu, K.: High resolution
8 atmospheric inversion of urban CO₂ emissions during the dormant season of the
9 Indianapolis Flux Experiment (INFLUX), Journal of Geophysical Research:
10 Atmospheres, *accepted*.
- 11 Law, R. M., Rayner, P. J., Steele, L. P., and Enting, I. G.: Data and modelling
12 requirements for CO₂ inversions using high-frequency data, Tellus B, 55, 512-521,
13 10.1034/j.1600-0889.2003.00029.x, 2003.
- 14 Law, R. M., Peters, W., Rödenbeck, C., Aulagnier, C., Baker, I., Bergmann, D. J.,
15 Bousquet, P., Brandt, J., Bruhwiler, L., Cameron-Smith, P. J., Christensen, J. H., Delage,
16 F., Denning, A. S., Fan, S., Geels, C., Houweling, S., Imasu, R., Karstens, U., Kawa, S.
17 R., Kleist, J., Krol, M. C., Lin, S. J., Lokupitiya, R., Maki, T., Maksyutov, S., Niwa, Y.,
18 Onishi, R., Parazoo, N., Patra, P. K., Pieterse, G., Rivier, L., Satoh, M., Serrar, S.,
19 Taguchi, S., Takigawa, M., Vautard, R., Vermeulen, A. T., and Zhu, Z.: TransCom model
20 simulations of hourly atmospheric CO₂: Experimental overview and diurnal cycle results
21 for 2002, Global Biogeochemical Cycles, 22, n/a-n/a, 10.1029/2007GB003050, 2008.
- 22 Le Quéré, C., Peters, G. P., Andres, R. J., Andrew, R. M., Boden, T. A., Ciais, P.,
23 Friedlingstein, P., Houghton, R. A., Marland, G., Moriarty, R., Sitch, S., Tans, P., Arneth,
24 A., Arvanitis, A., Bakker, D. C. E., Bopp, L., Canadell, J. G., Chini, L. P., Doney, S. C.,
25 Harper, A., Harris, I., House, J. I., Jain, A. K., Jones, S. D., Kato, E., Keeling, R. F.,
26 Klein Goldewijk, K., Körtzinger, A., Koven, C., Lefèvre, N., Maignan, F., Omar, A.,
27 Ono, T., Park, G. H., Pfeil, B., Poulter, B., Raupach, M. R., Regnier, P., Rödenbeck, C.,
28 Saito, S., Schwinger, J., Segschneider, J., Stocker, B. D., Takahashi, T., Tilbrook, B., van
29 Heuven, S., Viovy, N., Wanninkhof, R., Wiltshire, A., and Zaehle, S.: Global carbon
30 budget 2013, Earth Syst. Sci. Data, 6, 235-263, 10.5194/essd-6-235-2014, 2014.



- 1 Levin, I., Kromer, B., Schmidt, M., and Sartorius, H.: A novel approach for independent
2 budgeting of fossil fuel CO₂ over Europe by 14CO₂ observations, *Geophysical Research*
3 *Letters*, 30, n/a-n/a, 10.1029/2003GL018477, 2003.
- 4 Lu, R., and Turco, R. P.: Air pollutant transport in a coastal environment—II. Three-
5 dimensional simulations over Los Angeles basin, *Atmospheric Environment*, 29, 1499-
6 1518, [http://dx.doi.org/10.1016/1352-2310\(95\)00015-Q](http://dx.doi.org/10.1016/1352-2310(95)00015-Q), 1995.
- 7 Mahadevan, P., Wofsy, S. C., Matross, D. M., Xiao, X., Dunn, A. L., Lin, J. C., Gerbig,
8 C., Munger, J. W., Chow, V. Y., and Gottlieb, E. W.: A satellite-based biosphere
9 parameterization for net ecosystem CO₂ exchange: Vegetation Photosynthesis and
10 Respiration Model (VPRM), *Global Biogeochemical Cycles*, 22, GB2005,
11 10.1029/2006GB002735, 2008.
- 12 Description of the modifications made in WRF.3.1 and short user's manual of BEP,
13 2009.
- 14 Mesinger, F., DiMego, G., Kalnay, E., Mitchell, K., Shafran, P. C., Ebisuzaki, W., Jović,
15 D., Woollen, J., Rogers, E., Berbery, E. H., Ek, M. B., Fan, Y., Grumbine, R., Higgins,
16 W., Li, H., Lin, Y., Manikin, G., Parrish, D., and Shi, W.: North American Regional
17 Reanalysis, *Bulletin of the American Meteorological Society*, 87, 343-360,
18 10.1175/BAMS-87-3-343, 2006.
- 19 Miller, J. B., Lehman, S. J., Montzka, S. A., Sweeney, C., Miller, B. R., Karion, A.,
20 Wolak, C., Dlugokencky, E. J., Southon, J., Turnbull, J. C., and Tans, P. P.: Linking
21 emissions of fossil fuel CO₂ and other anthropogenic trace gases using atmospheric
22 14CO₂, *Journal of Geophysical Research: Atmospheres*, 117, n/a-n/a,
23 10.1029/2011JD017048, 2012.
- 24 Nakanishi, M., and Niino, H.: An Improved Mellor–Yamada Level-3 Model: Its
25 Numerical Stability and Application to a Regional Prediction of Advection Fog,
26 *Boundary-Layer Meteorol*, 119, 397-407, 10.1007/s10546-005-9030-8, 2006.
- 27 Nehr Korn, T., Henderson, J., Leidner, M., Mountain, M., Eluszkiewicz, J., McKain, K.,
28 and Wofsy, S.: WRF Simulations of the Urban Circulation in the Salt Lake City Area for
29 CO₂ Modeling, *Journal of Applied Meteorology and Climatology*, 52, 323-340,



- 1 10.1175/JAMC-D-12-061.1, 2012.
- 2 Newman, S., Xu, X., Affek, H. P., Stolper, E., and Epstein, S.: Changes in mixing ratio
3 and isotopic composition of CO₂ in urban air from the Los Angeles basin, California,
4 between 1972 and 2003, *Journal of Geophysical Research: Atmospheres*, 113, n/a-n/a,
5 10.1029/2008JD009999, 2008.
- 6 Newman, S., Jeong, S., Fischer, M. L., Xu, X., Haman, C. L., Lefer, B., Alvarez, S.,
7 Rappenglueck, B., Kort, E. A., Andrews, A. E., Peischl, J., Gurney, K. R., Miller, C. E.,
8 and Yung, Y. L.: Diurnal tracking of anthropogenic CO₂ emissions in the Los Angeles
9 basin megacity during spring 2010, *Atmos. Chem. Phys.*, 13, 4359-4372, 10.5194/acp-
10 13-4359-2013, 2013.
- 11 Newman, S., Xu, X., Gurney, K. R., Hsu, Y. K., Li, K. F., Jiang, X., Keeling, R. F., Feng,
12 S., O'Keefe, D., Patarasuk, R., Wong, K. W., Rao, P., Fisher, M. L., and Yung, Y. L.:
13 Toward consistency between bottom-up CO₂ emissions trends and top-down atmospheric
14 measurements in the Los Angeles megacity, *Atmos. Chem. Phys. Discuss.*, 1-45,
15 10.5194/acpd-15-1-2015, 2015.
- 16 Pataki, D. E., Alig, R. J., Fung, A. S., Golubiewski, N. E., Kennedy, C. A., McPherson,
17 E. G., Nowak, D. J., Pouyat, R. V., and Romero Lankao, P.: Urban ecosystems and the
18 North American carbon cycle, *Global Change Biology*, 12, 2092-2102, 10.1111/j.1365-
19 2486.2006.01242.x, 2006.
- 20 Pataki, D. E., Xu, T., Luo, Y. Q., and Ehleringer, J. R.: Inferring biogenic and
21 anthropogenic carbon dioxide sources across an urban to rural gradient, *Oecologia*, 152,
22 307-322, 10.1007/s00442-006-0656-0, 2007.
- 23 Pillai, D., Gerbig, C., Marshall, J., Ahmadov, R., Kretschmer, R., Koch, T., and Karstens,
24 U.: High resolution modeling of CO₂ over Europe: implications for representation errors
25 of satellite retrievals, *Atmos. Chem. Phys.*, 10, 83-94, 10.5194/acp-10-83-2010, 2010.
- 26 Pillai, D., Gerbig, C., Ahmadov, R., Rödenbeck, C., Kretschmer, R., Koch, T.,
27 Thompson, R., Neininger, B., and Lavrié, J. V.: High-resolution simulations of
28 atmospheric CO₂ over complex terrain – representing the Ochsenkopf mountain tall
29 tower, *Atmos. Chem. Phys.*, 11, 7445-7464, 10.5194/acp-11-7445-2011, 2011.



- 1 Rao, P., Gurney, K. R., Patarasuk, R., Song, Y., Miller, C. E., Duren, R. M., and
2 Eldering, A.: Spatio-temporal Variations in Onroad Vehicle Fossil Fuel CO₂ Emissions
3 in the Los Angeles Megacity, *Environmental Science and Technology*, submitted, 2015.
- 4 Riley, W. J., Hsueh, D. Y., Randerson, J. T., Fischer, M. L., Hatch, J. G., Pataki, D. E.,
5 Wang, W., and Gouliden, M. L.: Where do fossil fuel carbon dioxide emissions from
6 California go? An analysis based on radiocarbon observations and an atmospheric
7 transport model, *Journal of Geophysical Research: Biogeosciences*, 113, n/a-n/a,
8 10.1029/2007JG000625, 2008.
- 9 Rödenbeck, C., Gerbig, C., Trusilova, K., and Heimann, M.: A two-step scheme for high-
10 resolution regional atmospheric trace gas inversions based on independent models,
11 *Atmos. Chem. Phys.*, 9, 5331-5342, 10.5194/acp-9-5331-2009, 2009.
- 12 Rogers, R. E., Deng, A., Stauffer, D. R., Gaudet, B. J., Jia, Y., Soong, S.-T., and
13 Tanrikulu, S.: Application of the Weather Research and Forecasting Model for Air
14 Quality Modeling in the San Francisco Bay Area, *Journal of Applied Meteorology and
15 Climatology*, 52, 1953-1973, 10.1175/JAMC-D-12-0280.1, 2013.
- 16 Ryerson, T. B., Andrews, A. E., Angevine, W. M., Bates, T. S., Brock, C. A., Cairns, B.,
17 Cohen, R. C., Cooper, O. R., de Gouw, J. A., Fehsenfeld, F. C., Ferrare, R. A., Fischer,
18 M. L., Flagan, R. C., Goldstein, A. H., Hair, J. W., Hardesty, R. M., Hostetler, C. A.,
19 Jimenez, J. L., Langford, A. O., McCauley, E., McKeen, S. A., Molina, L. T., Nenes, A.,
20 Oltmans, S. J., Parrish, D. D., Pederson, J. R., Pierce, R. B., Prather, K., Quinn, P. K.,
21 Seinfeld, J. H., Senff, C. J., Sorooshian, A., Stutz, J., Surratt, J. D., Trainer, M.,
22 Volkamer, R., Williams, E. J., and Wofsy, S. C.: The 2010 California Research at the
23 Nexus of Air Quality and Climate Change (CalNex) field study, *Journal of Geophysical
24 Research: Atmospheres*, 118, 5830-5866, 10.1002/jgrd.50331, 2013.
- 25 Sarrat, C., Noilhan, J., Dolman, A. J., Gerbig, C., Ahmadov, R., Tolk, L. F., Meesters, A.
26 G. C. A., Hutjes, R. W. A., Ter Maat, H. W., Pérez-Landa, G., and Donier, S.:
27 Atmospheric CO₂ modeling at the regional scale: an intercomparison of 5 meso-scale
28 atmospheric models, *Biogeosciences*, 4, 1115-1126, 10.5194/bg-4-1115-2007, 2007.
- 29 Scarino, A. J., Obland, M. D., Fast, J. D., Burton, S. P., Ferrare, R. A., Hostetler, C. A.,



- 1 Berg, L. K., Lefer, B., Haman, C., Hair, J. W., Rogers, R. R., Butler, C., Cook, A. L., and
2 Harper, D. B.: Comparison of mixed layer heights from airborne high spectral resolution
3 lidar, ground-based measurements, and the WRF-Chem model during CalNex and
4 CARES, Atmos. Chem. Phys. Discuss., 13, 13721-13772, 10.5194/acpd-13-13721-2013,
5 2013.
- 6 Strong, C., Stwertka, C., Bowling, D. R., Stephens, B. B., and Ehleringer, J. R.: Urban
7 carbon dioxide cycles within the Salt Lake Valley: A multiple-box model validated by
8 observations, Journal of Geophysical Research: Atmospheres, 116, n/a-n/a,
9 10.1029/2011JD015693, 2011.
- 10 Tarantola, A.: Inverse problem theory and methods for model parameter estimation,
11 Book, Whole, Society for Industrial and Applied Mathematics, Philadelphia, PA, 2005.
- 12 Turnbull, J., Rayner, P., Miller, J., Naegler, T., Ciais, P., and Cozic, A.: On the use of
13 $^{14}\text{CO}_2$ as a tracer for fossil fuel CO_2 : Quantifying uncertainties using an atmospheric
14 transport model, Journal of Geophysical Research: Atmospheres, 114, n/a-n/a,
15 10.1029/2009JD012308, 2009.
- 16 Turnbull, J. C., Miller, J. B., Lehman, S. J., Tans, P. P., Sparks, R. J., and Southon, J.:
17 Comparison of $^{14}\text{CO}_2$, CO, and SF₆ as tracers for recently added fossil fuel CO₂ in the
18 atmosphere and implications for biological CO₂ exchange, Geophysical Research
19 Letters, 33, n/a-n/a, 10.1029/2005GL024213, 2006.
- 20 Turnbull, J. C., Karion, A., Fischer, M. L., Faloona, I., Guilderson, T., Lehman, S. J.,
21 Miller, B. R., Miller, J. B., Montzka, S., Sherwood, T., Saripalli, S., Sweeney, C., and
22 Tans, P. P.: Assessment of fossil fuel carbon dioxide and other anthropogenic trace gas
23 emissions from airborne measurements over Sacramento, California in spring 2009,
24 Atmos. Chem. Phys., 11, 705-721, 10.5194/acp-11-705-2011, 2011.
- 25 Ulrickson, B. L., and Mass, C. F.: Numerical Investigation of Mesoscale Circulations
26 over the Los Angeles Basin. Part II: Synoptic Influences and Pollutant Transport,
27 Monthly Weather Review, 118, 2162-2184, 10.1175/1520-
28 0493(1990)118<2162:NIOMCO>2.0.CO;2, 1990.
- 29 UN: World Urbanization Prospects e Revision 2005, Factsheet 7: Mega-cities, 2006.



- 1 United Nations, Department of Economic and Social Affairs, Population Division. World
2 Urbanization Prospects: The 2005 Revision. Working Paper No. ESA/P/WP/200, 2006.
- 3 UN: World Urbanization Prospects: The 2009 Revision, 2010.
- 4 Wennberg, P. O., Mui, W., Wunch, D., Kort, E. A., Blake, D. R., Atlas, E. L., Santoni, G.
5 W., Wofsy, S. C., Diskin, G. S., Jeong, S., and Fischer, M. L.: On the Sources of
6 Methane to the Los Angeles Atmosphere, *Environmental Science & Technology*, 46,
7 9282-9289, 10.1021/es301138y, 2012.
- 8 Wong, K. W., Fu, D., Pongetti, T. J., Newman, S., Kort, E. A., Duren, R., Hsu, Y. K.,
9 Miller, C. E., Yung, Y. L., and Sander, S. P.: Mapping CH₄ : CO₂ ratios in Los Angeles
10 with CLARS-FTS from Mount Wilson, California, *Atmos. Chem. Phys.*, 15, 241-252,
11 10.5194/acp-15-241-2015, 2015.
- 12 Wu, L., Bocquet, M., Lauvaux, T., Chevallier, F., Rayner, P., and Davis, K.: Optimal
13 representation of source-sink fluxes for mesoscale carbon dioxide inversion with
14 synthetic data, *Journal of Geophysical Research: Atmospheres*, 116, n/a-n/a,
15 10.1029/2011JD016198, 2011.
- 16 Wunch, D., Wennberg, P. O., Toon, G. C., Keppel-Aleks, G., and Yavin, Y. G.:
17 Emissions of greenhouse gases from a North American megacity, *Geophysical Research*
18 *Letters*, 36, L15810, 10.1029/2009GL039825, 2009.
- 19 Xiao, X., Hollinger, D., Aber, J., Goltz, M., Davidson, E. A., Zhang, Q., and Moore Iii,
20 B.: Satellite-based modeling of gross primary production in an evergreen needleleaf
21 forest, *Remote Sensing of Environment*, 89, 519-534,
22 <http://dx.doi.org/10.1016/j.rse.2003.11.008>, 2004.
- 23 Yver, C. E., Graven, H. D., Lucas, D. D., Cameron-Smith, P. J., Keeling, R. F., and
24 Weiss, R. F.: Evaluating transport in the WRF model along the California coast, *Atmos.*
25 *Chem. Phys.*, 13, 1837-1852, 10.5194/acp-13-1837-2013, 2013.
- 26 Zhou, Y., and Gurney, K.: A new methodology for quantifying on-site residential and
27 commercial fossil fuel CO₂ emissions at the building spatial scale and hourly time scale,
28 *Carbon Management*, 1, 45-56, 10.4155/cmt.10.7, 2010.
- 29



Table 1. Common elements of the WRF-Chem configuration used in all runs.

Option	Description
Microphysics	WSM5 (Hong et al., 2004)
Longwave radiation	RRTMG (Iacono et al., 2008)
Shortwave radiation	RRTMG (Iacono et al., 2008)
Land surface	Noah land surface model (Chen and Dudhia, 2001)
Cumulus scheme	Grell-3 (Grell and Dévényi, 2002) applied to 12-km domain (d01) only

1

2



Table 2. WRF configurations used for the sensitivity runs.

Configuration	PBL scheme	Urban surface scheme	Grid spacing (km)
BouLac_BEP_d02	BouLac	BEP	4
BouLac_BEP_d03	BouLac	BEP	1.3
BouLac_UCM_d02	BouLac	UCM	4
BouLac_UCM_d03	BouLac	UCM	1.3
MYJ_d02	MYJ	None	4
MYN_d03	MYJ	None	1.3
MYJ_UCM_d02	MYJ	UCM	4
MYJ_UCM_d03	MYJ	UCM	1.3
MYNN_d02	MYNN	None	4
MYNN_d03	MYNN	None	1.3
MYNN_UCM_d02	MYNN	UCM	4
MYNN_UCM_d03	MYNN	UCM	1.3

1

2



Table 3. Locations of the 2015-era GHG measurement sites in the model domain[‡]

Code*	Name	Type	Lat. (° N)	Lon. (° E)
GH	Granada Hills	Tower	34.28	-118.47
Pasadena	Pasadena	Building top	34.14	-118.13
MWO	Mt. Wilson	Mountain top	34.22	-118.06
USC	University of South California	Building top	34.02	-118.29
Compton	Compton	Tower	33.87	-118.28
CSUF	California State University, Fullerton	Building top	33.88	-117.88
Ontario	Ontario	Tower	34.06	-117.58
SB	San Bernardino	Tower	34.09	-118.35
Dryden [†]	Dryden	TCCON	34.95	-117.89
VV	Victorville	Tower	34.61	-117.29
UCI	University of California, Irvine	Building top	33.64	-117.84
SCI	San Clemente Island	Tower	32.92	-118.49
PV	Palos Verdes	In-situ non-standard	33.74	-118.35

[‡]La Jolla site is operating but not included in this paper

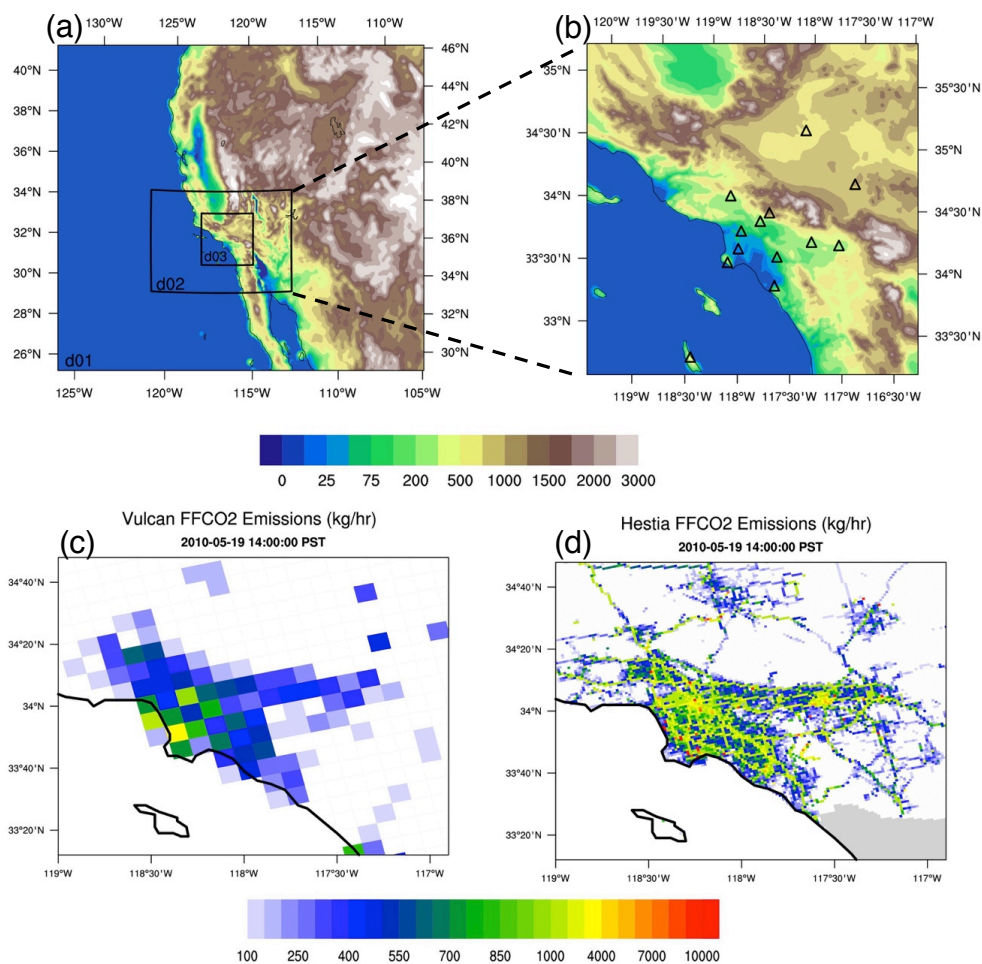
*Codes used in this paper

[†] In the analysis, we assume Dryden site is a near-surface point measurement like other sites rather than a column observation for simplicity.

1

2

3



1

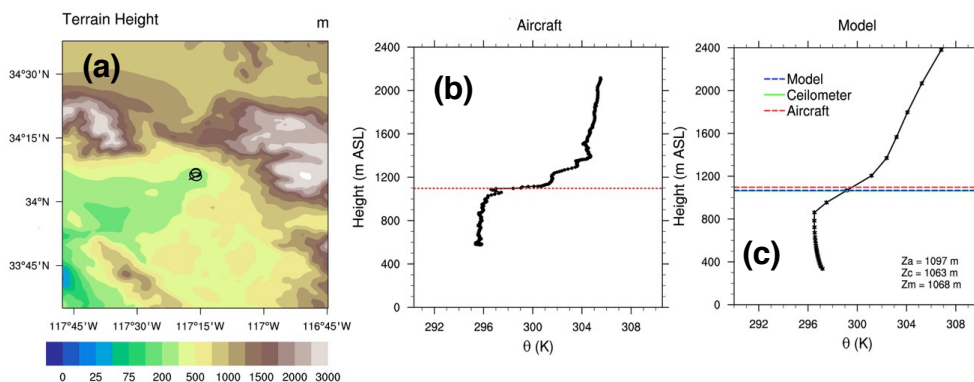
2

3 Figure 1. (a) Model domains. Contours are terrain height (unit: m). (b) The 1.3-km
4 model domain (d03) and terrain height (unit: m). Triangles represent the locations of the
5 GHG measurement sites. (c and d) Snapshots of the Vulcan and Hestia FFCO₂ emissions
6 (unit: kg/hr) over the LA megacity at 14:00 PST on 15 May 2010.

7



1



2

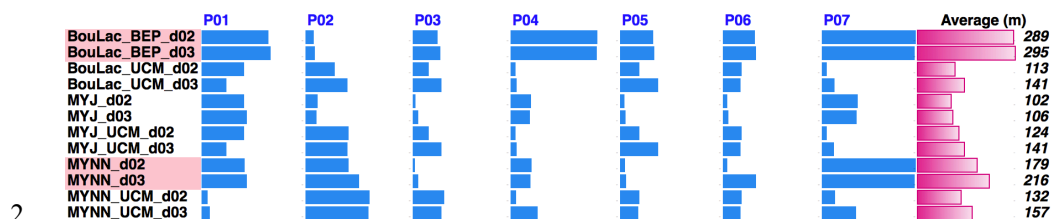
3

4 Figure 2. A case selected on 19 May 2010 at 12:25 (PST) (a) Location of the vertical
5 profile flown by the CalNex aircraft and the neighbouring terrain heights (units: m). (b)
6 In-situ potential temperature profile measured by the aircraft . The red dashed line at
7 ~1100 m is the PBL height calculated based on the vertical gradient of potential
8 temperature Θ (K). (c) Modelled potential temperature profile from the
9 MYNN_UCM_d02 configuration. The red dashed line is the aircraft-determined PBL
10 height (Z_a in masl). The solid green line is the PBL height measured by the Caltech
11 ceilometer (Z_c in masl). The blue line is the modelled PBL height (Z_m in m).

12



1



2

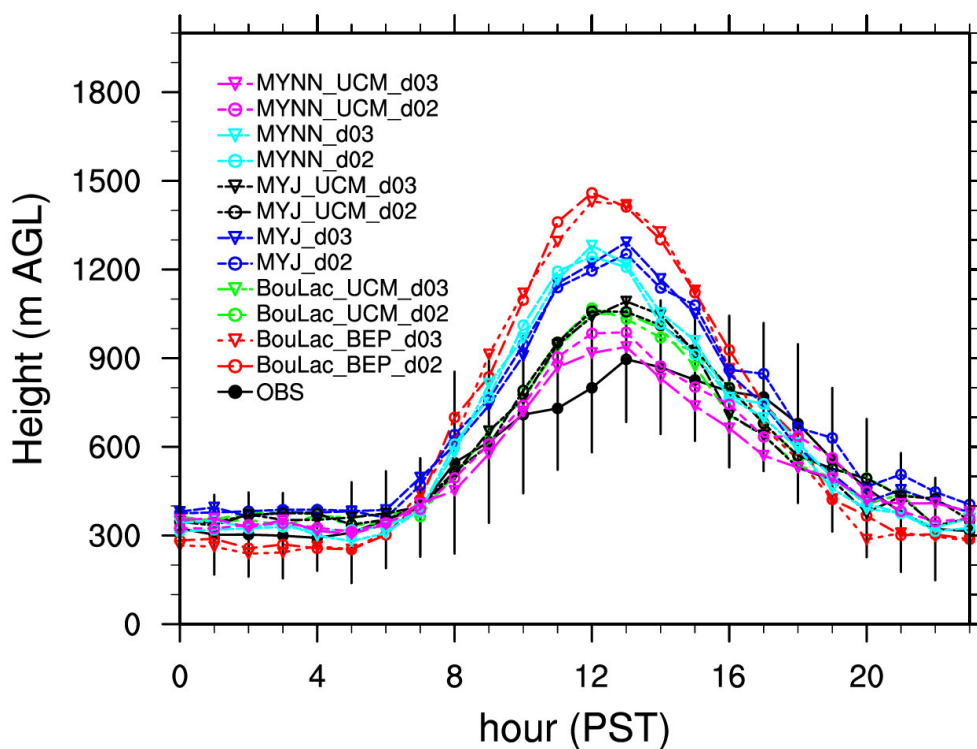
3

4 Figure 3. Absolute difference between the aircraft-determined and modelled PBL height
 5 for each profile: P01, P02, ..., and P07 (blue bars). The pink bars in the last column
 6 represent the averaged bias over all of the profiles for each configuration. Note that the
 7 shorter the bar is, the better agreement the model has with the observations.

8

9

10

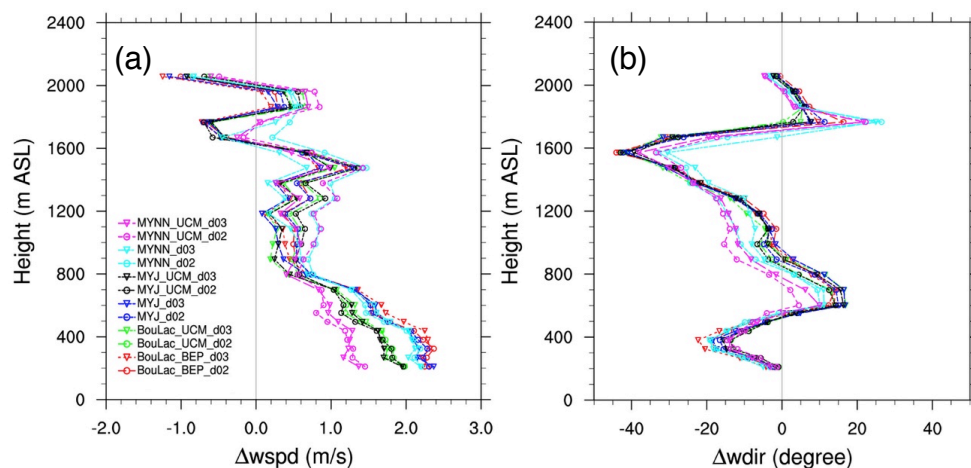


1

2

3 Figure 4. Average diurnal variation of the ceilometer-measured and modelled PBL
4 heights at California Institute of Technology (Caltech) in Pasadena, CA during 15 May
5 through 15 June 2010. Error bars indicate standard deviations of the means of the
6 ceilometer measurement.

7



1

2

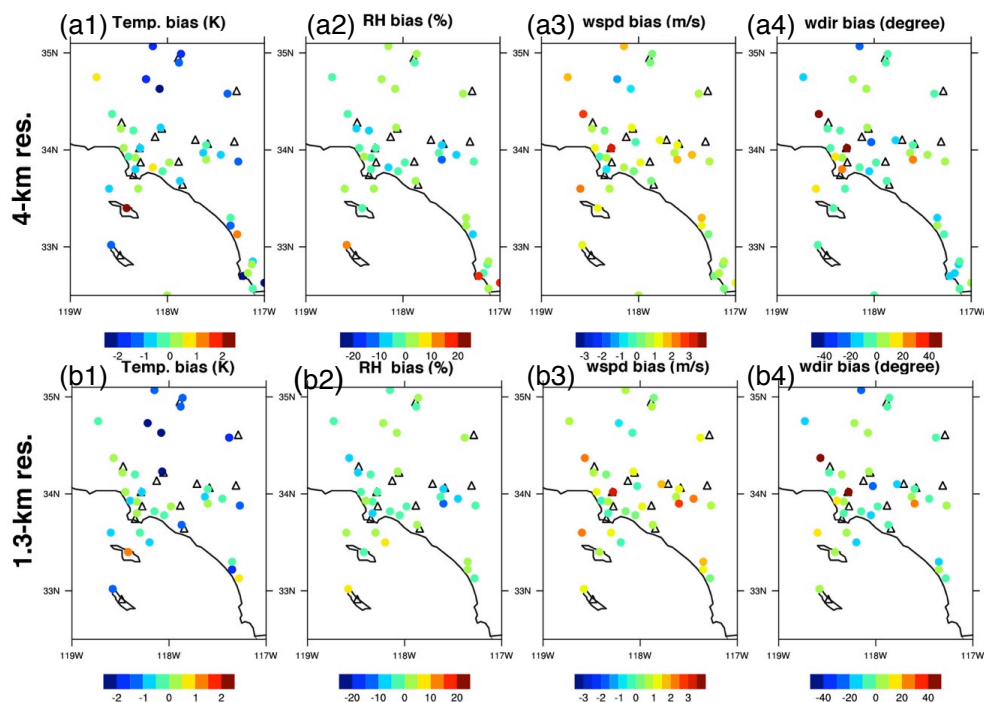
3 Figure 5. Average differences of wind profiles between the simulations and observations
4 (model – wind radar profiler) at the Los Angeles International Airport (LAX). (a) The
5 difference for wind speed (unit: m/s); (b) for wind direction (unit: degree).

6

7



1
2



3

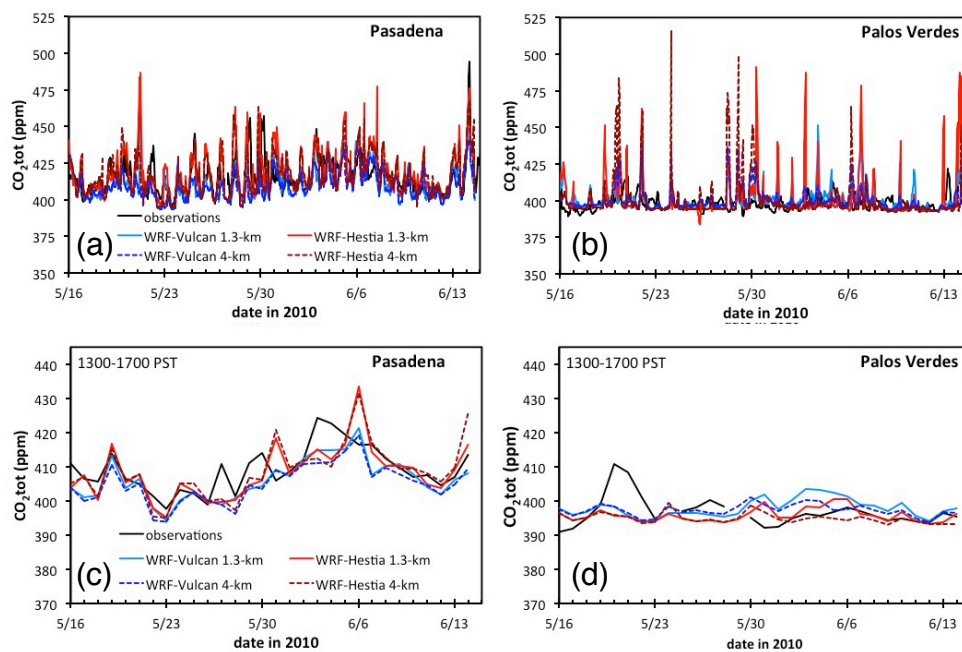
4 Figure 6. Bias maps of the MYNN_UCM runs versus National Weather Stations (NWS)
5 over the LA megacity (Model – NWS): (a1-a4) 4-km run; (b1 – b4) 1.3-km run. Black
6 triangles indicate the locations of the GHG measurement sites.

7

8



1



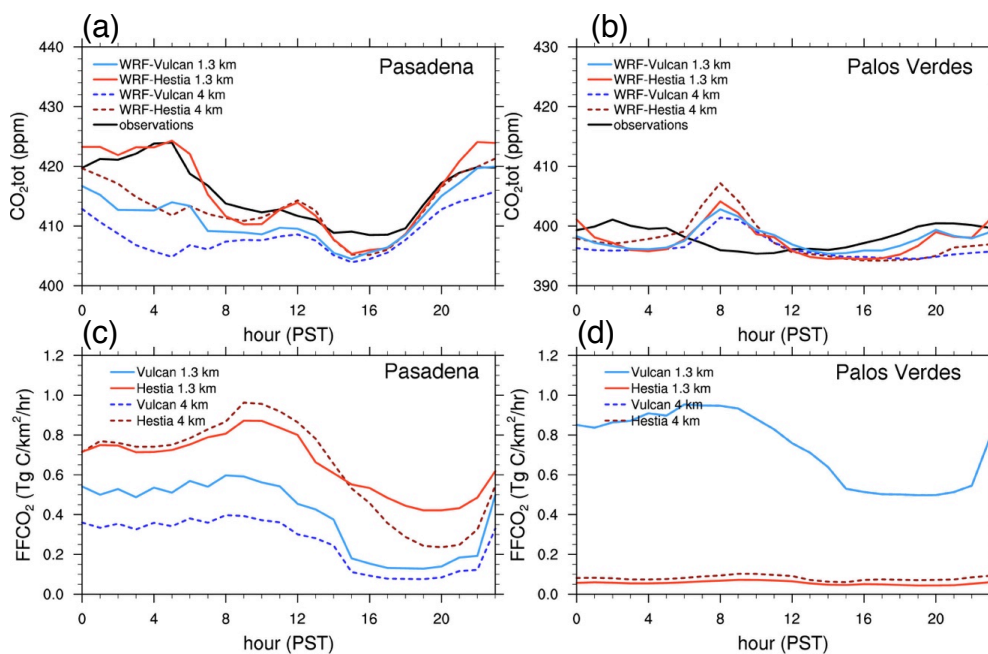
2

3 Figure 7. Comparison of the observed and modelled CO₂ concentrations at the (a and c)
4 Pasadena and (b and d) Palos Verdes sites: (a and b) is hourly time series, (c and d) is
5 daily afternoon average over 1300 – 1700 PST.

6



1



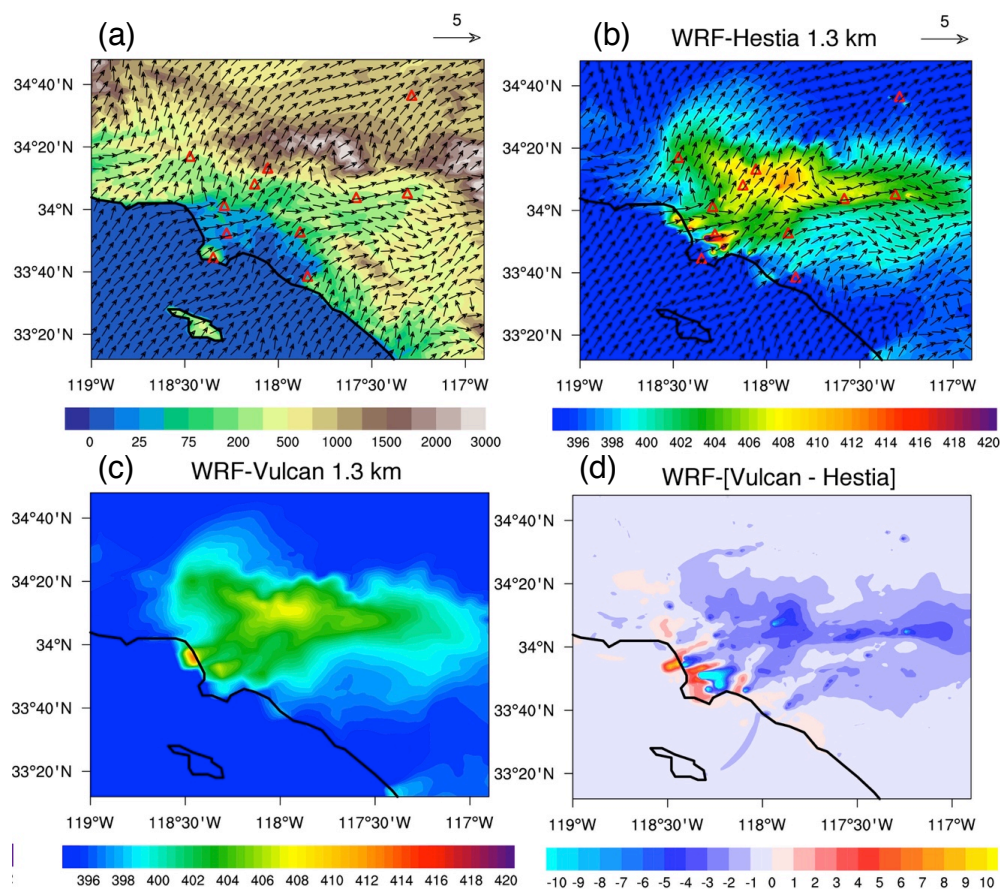
2

3 Figure 8. Averaged diurnal variation of observed and modelled CO₂ concentration and
4 FFCO₂ emissions for the (a and c) Pasadena and (b and d) Palos Verdes sites during
5 CalNex-LA.

6

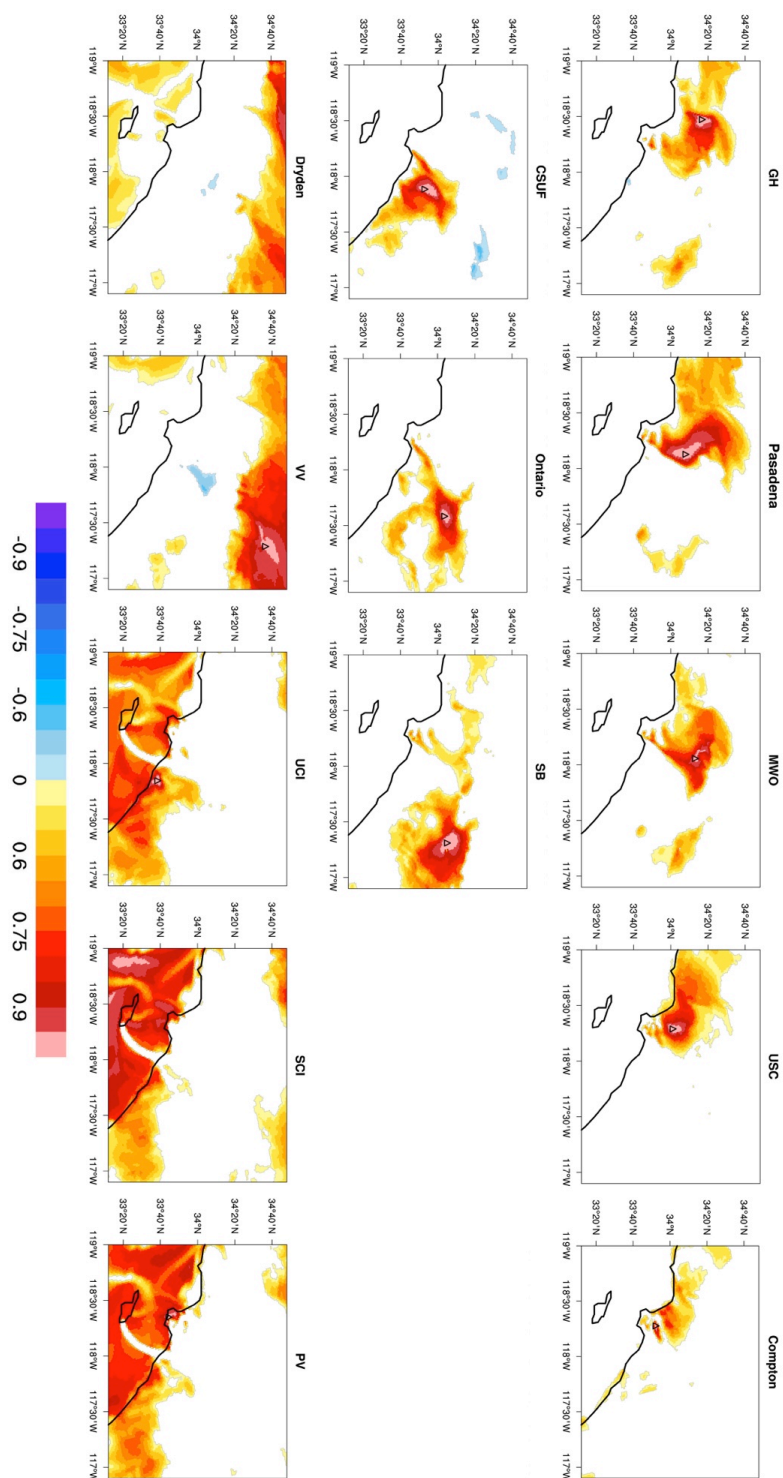


1



2

3 Figure 9. (a and b) The first empirical orthogonal function (EOF 1) for the surface wind
4 pattern simulated by MYNN_UCM_d03 at 1400 PST during CalNex-LA. EOF 1
5 accounts for 48.1 % of the variance in the average winds. Contours: (a) terrain height
6 (unit: m); (b) the modelled surface CO₂ concentration (unit: ppm) from the 1.3-km WRF-
7 Hestia run. The red triangles indicate the locations of the GHG measurement sites. (c)
8 The modelled CO₂ concentration from the 1.3-km WRF-Vulcan run (unit: ppm). (d) The
9 difference of the modelled CO₂ concentration between the 1.3-km WRF-Hestia and
10 WRF-Vulcan runs (unit: ppm).

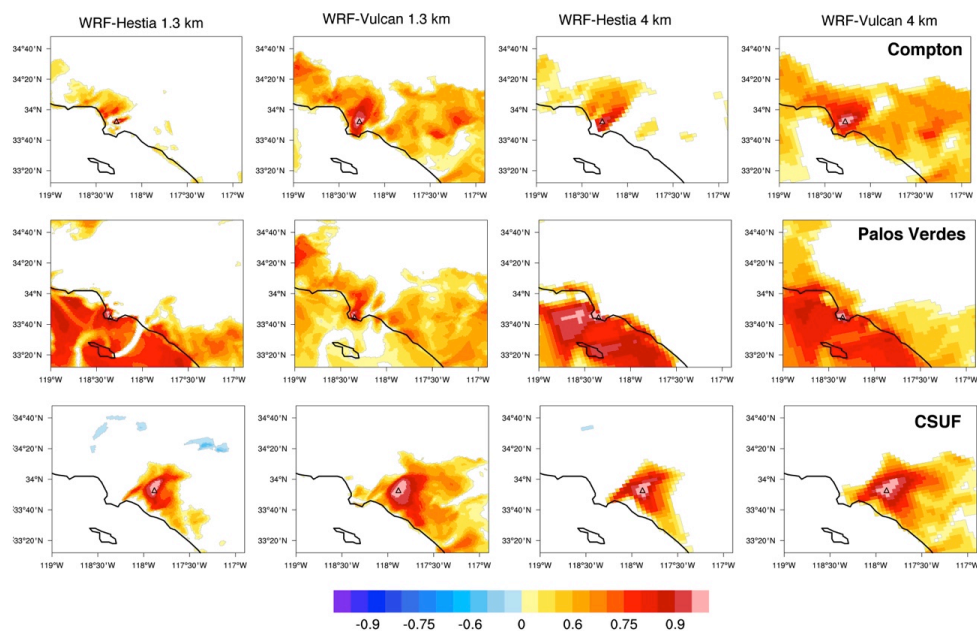




1 Figure 10. The spatial correlation map (R) of the 1.3-km WRF-Hestia simulated CO_2
2 concentration between each site and the remainder of the domain at 1400 PST during the
3 CalNex-LA campaign. The correlation map was constructed by calculating the
4 simultaneous correlation of the site CO_2 to the CO_2 over rest of the LA megacity. Note
5 that only those pixels that pass the t -test at the significance level of 0.01 ($|R| \geq 0.46$) are
6 coloured.



1

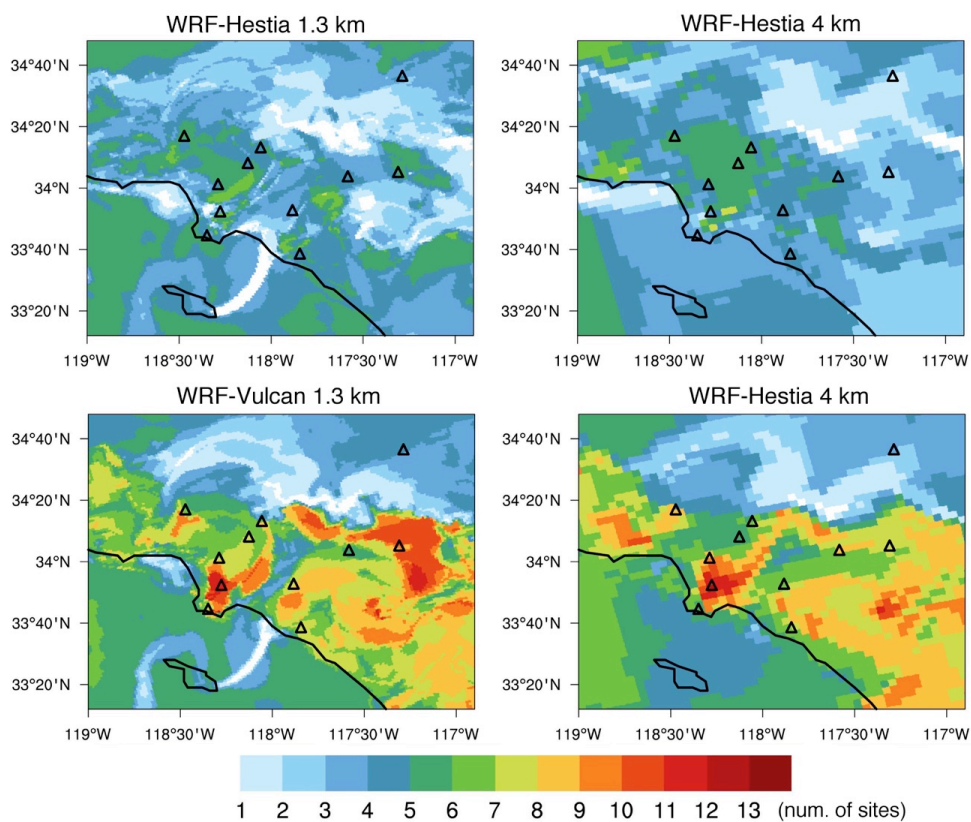


2

3 Figure 11. Same as Figure 10 but for the Compton (upper row), Palos Verdes (middle
4 row), and CSUF (lower row) sites only. Shown are the correlation maps of these three
5 measurement sites for the 1.3-km WRF-Hestia (first column), 1.3-km WRF-Vulcan
6 (second column), 4-km WRF-Hestia (third column), and 4-km WRF-Vulcan runs. Note
7 that only those pixels that pass the t -test at the significance level of 0.01 ($|R| \geq 0.46$) are
8 coloured.



1



2

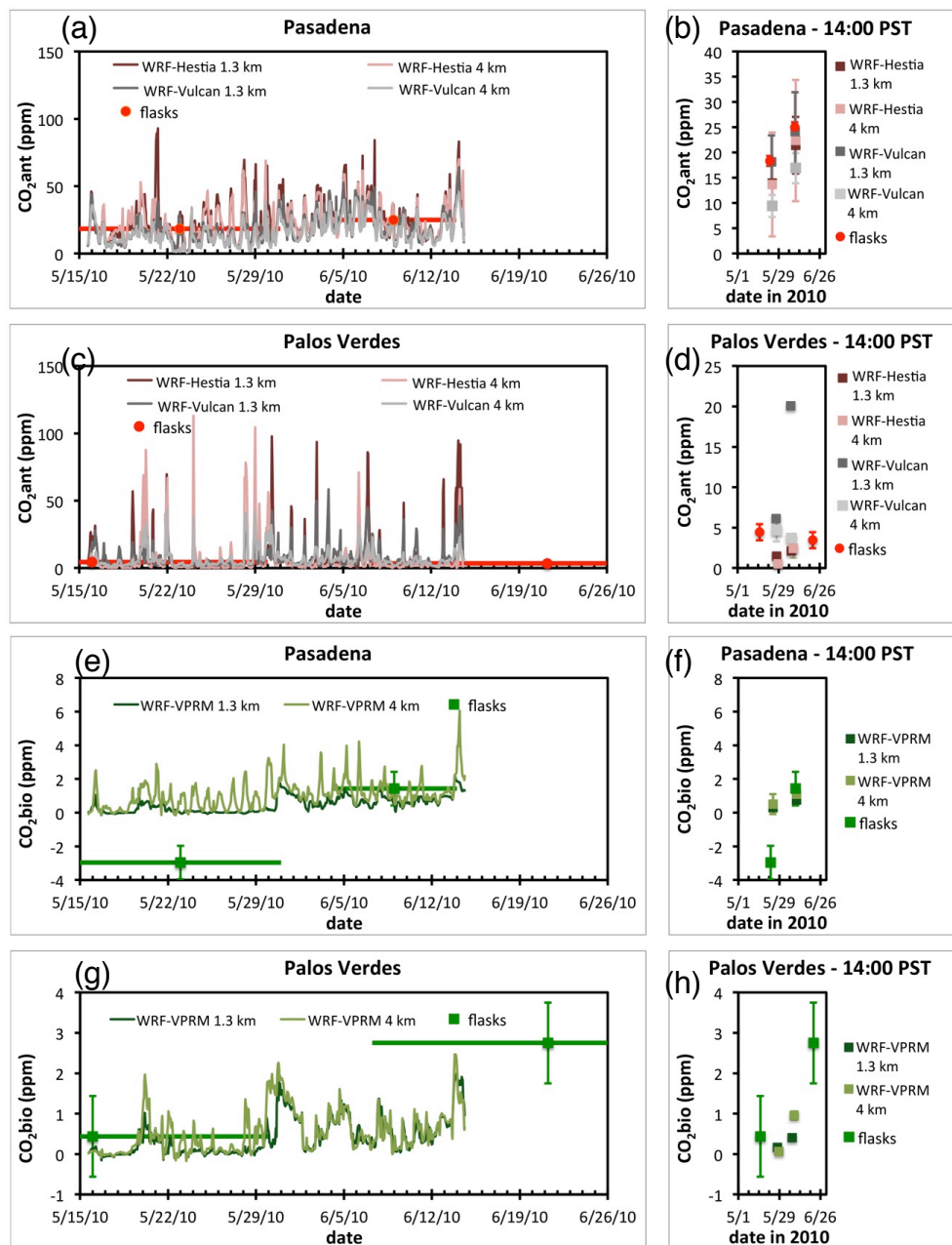
3 Figure 12. The composite maps of spatial correlation (R in Figure 10 and 11) for the 1.3-
4 km WRF-Hestia, 1.3-km WRF-Vulcan, 4-km WRF-Hestia, and 4-km WRF-Vulcan runs.
5 The composite map was constructed by determining the number of the observation sites
6 for which $|R|$ is greater than 0.46 at each grid cell. $|R| = 0.46$ is the critical value at the
7 significance level of 0.01 of t -test. Specifically, white cells indicate that no sites are
8 correlated well at the location; dark red cells indicate that over 13 sites have good
9 correlation at the location. The SCI and Dryden sites are not shown on these maps.

10

11

12

13



1

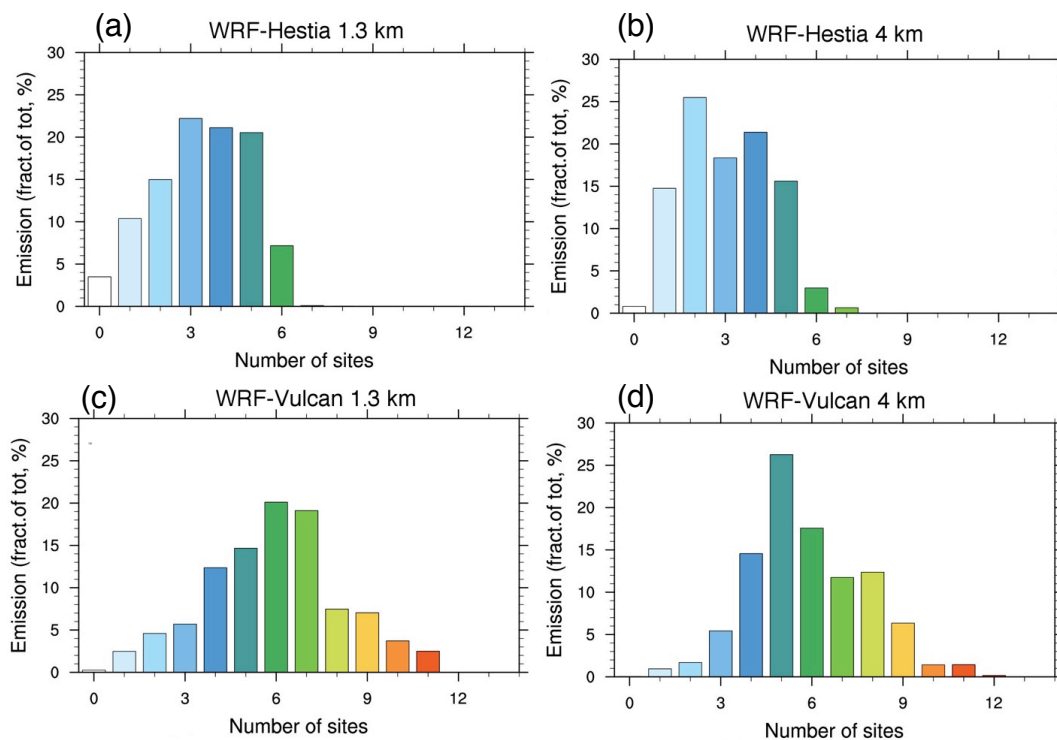
2 Figure 13. Comparisons of flask-sampled and modelled (a-d) anthropogenic fossil fuel
3 and (e-h) biogenic CO₂ concentration. Left column: hourly time series. The horizontal
4 error bars on the flask-sampled data points indicate the range of dates combined in each
5 sample. Note that much of the time periods for the $\Delta^{14}\text{C}$ samples at the Palos Verdes site



- 1 are before or after the modelling period. Right column: Averages at 1400 PST during
- 2 CalNex-LA. See Newman et al. (2015) for details about the sites and sampling
- 3 information.



1



2

3 Figure 14. The fraction of the FFCO₂ emission over the LA megacity as function of the number
4 of the GHG measurement sites that covers the area for (a) 1.3-km WRF-Hestia, (b) 4-km WRF-
5 Hestia, (c) 1.3-km WRF-Vulcan, and (d) 4-km WRF-Vulcan runs during CalNex-LA.

6